



Agenzia nazionale per le nuove tecnologie, l'energia
e lo sviluppo economico sostenibile



Ministero dello Sviluppo Economico

RICERCA DI SISTEMA ELETTRICO

Development of a multi-scale methodology for composite structural
modelling and validation of modelling procedure by mechanical testing -
Final Report

Andrea Moriani

Report RdS/2012/268

DEVELOPMENT OF A MULTI-SCALE METHODOLOGY FOR COMPOSITE STRUCTURAL MODELLING AND
VALIDATION OF MODELLING PROCEDURE BY MECHANICAL TESTING – FINAL REPORT

Andrea Moriani (ENEA)

Settembre 2012

Report Ricerca di Sistema Elettrico

Accordo di Programma Ministero dello Sviluppo Economico - ENEA

Area: Governo, gestione e sviluppo del sistema elettrico nazionale

Progetto: 1.3.2 Fusione nucleare: attività di fisica e tecnologia della fusione complementari a ITER

Responsabile del Progetto: Aldo Pizzuto, ENEA

Indice

| | |
|---|----|
| Sommario | 4 |
| 1. Introduction | 5 |
| 2. Method to represent the results about a progressive failure model in composite materials | 5 |
| 3. Selection of the environment for the development..... | 14 |
| 4. Constitutive model for a balanced plain weave fabric | 22 |
| 5. Validation of the model by testing | 47 |
| 6. Conclusions | 63 |
| Appendix 1 | 65 |
| <i>Classical laminate theory applied to tensile load tests</i> | 65 |
| REFERENCES..... | 72 |

Sommario

Objectives of the work are to develop a multiscale methodology for composite structural modelling and to validate the modelling procedure by mechanical testing.

In the field of the computational material science the multiscale methodology plays an important role. It is based on the hierarchical concept which recognises that there is a strong interconnection between phenomena which happen to different scales of length and time. In the field of the composite material the approach consists in the description of the ply by knowing the behaviour of the constituents, i.e. fibre and matrix.

In this work was developed a constitutive model for a balanced plain weave fabric. This model, starting from geometrical parameters and mechanical parameters of the single constituents (fibre and matrix), determines the effective moduli of the representative unit cell (RUC). This model was implemented into a general purpose finite element program ABAQUS, building a specific user subroutine.

The last part of this job was to determine a material failure mechanism theory for the balanced plain weave architecture that was implemented in the same specific user subroutine. The prediction of the failure at each increment of the load was obtained by using a quadratic failure criterion, applied to the strains with stiffness and strength reduction scheme to account for damage within the yarns.

This standard user subroutine is an augmentation for any commercial finite element code giving the possibility to deal with any composite material made with balanced plain weave fabric, knowing the mechanical properties of the single constituents and the specific failure mechanism.

1. Introduction

A technique to describe the mechanical behaviour of the composite materials is the multiscale methodology, which allows to link the macroscopic behaviour with the micro-structural characteristics and it results to be a more predictive approach (with respect to phenomenological models) with the possibility to estimate the effect of a change in the fibres and matrix arrangement on the composite behaviour. Practically, the approach consists in the description of the behaviour at the scale of the constituents, fibre and matrix, (microscale) where each constituent is modelled by using continuum mechanics relationships. Afterwards, the homogenisation treatment will allow to create a mesoscale structure (e.g., layer) and finally to deduce the macroscopic behaviour. The findings and results of this study can be implemented in a finite element code by means of a user subroutine. A similar approach can be attempted for thermal properties.

An important part of the task is the validation of the modelling by testing. These tests are aimed both at the determination of the basic constituent properties (fibre and matrix), fibre-matrix interface behaviour and at composite macroscopic properties. The tests include fibre tensile and composite tensile, compression, shear and bending.

2. Method to represent the results about a progressive failure model in composite materials

We have started to study the argument of the design of composite materials using a general purpose finite element program named ABAQUS. Laminated composite structures under load develop local failures such as matrix cracks, fiber breakage and fibre matrix debonds, which are termed as damage. These effects cause permanent loss of stiffness and strength of the material. It becomes important to predict the initiation and growth of such damage for assessing the performance of composite structures.

The analysis of composite laminates is complicated because of both material and geometric non-linearity, that came into play when the loads are increased beyond the first ply failure. Material non-linearity results from the damage mentioned early, and the geometric non-linearity is due to large displacements experienced by the structure during loading.

Commercial code gives to the user tools to deal with composite materials. For two-dimensional models there is shell element based on first order shear deformation theory, that have better performance in large deformation analysis. The strain state is referred to a specific coordinate system and the stacking sequence of the laminate is specified to this reference coordinate system.

As we have just said damage in composite materials plays an important role. To study these behaviours is used a progressive failure method, where the load is

applied incrementally during the analysis. At each load step, a geometric non-linear analysis is performed until a converged solution is obtained. Knowing the deformation and stress states at each material integration point, it become possible to compare these result with material allowable stress. If failure is detected, stiffness reduction is carried out at the integration Gauss points of the finite element mesh depending on the mode of failure. However, it is not an easy task to determine the degraded properties of the damaged material with certainty.

The user can define material properties as functions of the field variables at a material point using specific user subroutine.

The need to write specific software that represents an augmentation for any commercial finite element code, gives a big problem to the user in the representation of the results of the analysis. Where is the first ply failure and how the progression of the damage develops, these are some questions that the users have to answer.

In this paragraph is implemented a progressive failure method into the general purpose finite element program, ABAQUS. A specific application is developed for a post processing visualization of the results.

We have studied a panel, made of five unidirectional plies, where all the edges are clamped and the load is a uniform pressure applied to the bottom surface (Figure 2.1).

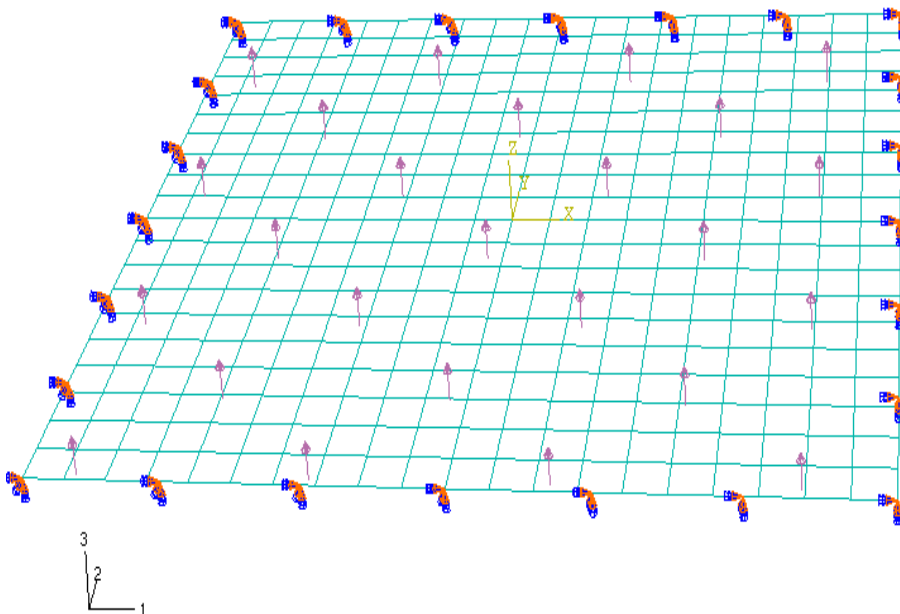


Figure 2.1: Plate geometry.

The plate specification is shown in Table 2.1 and the material properties are shown in Table 2.2. The orthotropic material properties of a lamina are obtained either by the theoretical approach or through suitable laboratory tests. The

theoretical approach, called a micromechanics approach, that relate the fiber and matrix contributions to the properties of complete structures.

Table 2.1: Laminate plate specifications

| Lay-up Sequence | Number of Plies | Length (mm) | Width (mm) | Thickness (mm) |
|-----------------|-----------------|-------------|------------|----------------|
| [0/45/90/-45/0] | 5 | 600 | 600 | 3.43 |

Table2.2: Mechanical properties of unidirectional E-Glass/Polyester ply

| | |
|--|-------|
| Longitudinal Modulus, E_x (GPa) | 23.6 |
| Transverse Modulus, $E_y = E_z$ (GPa) | 10.0 |
| Shear Modulus, G_{xy} (GPa) | 1.0 |
| Poisson's ratio, ν_{xy} | 0.23 |
| Longitudinal Tensile Strength, X_T (MPa) | 735.0 |
| Longitudinal Compressive Strength, X_C (MPa) | 600.0 |
| Transverse Tensile Strength, Y_T (MPa) | 45.0 |
| Transverse Compressive Strength, Y_C (MPa) | 100.0 |
| In-Plane Shear Strength, SC (MPa) | 45.0 |

A typical procedure for a progressive failure analysis is illustrated in figure 2.2. The preprocessing phase is built in the standard ABAQUS environmental and a specific user subroutine USDFLD was written, which allows the user to define material properties as functions of the field variables at a material point.

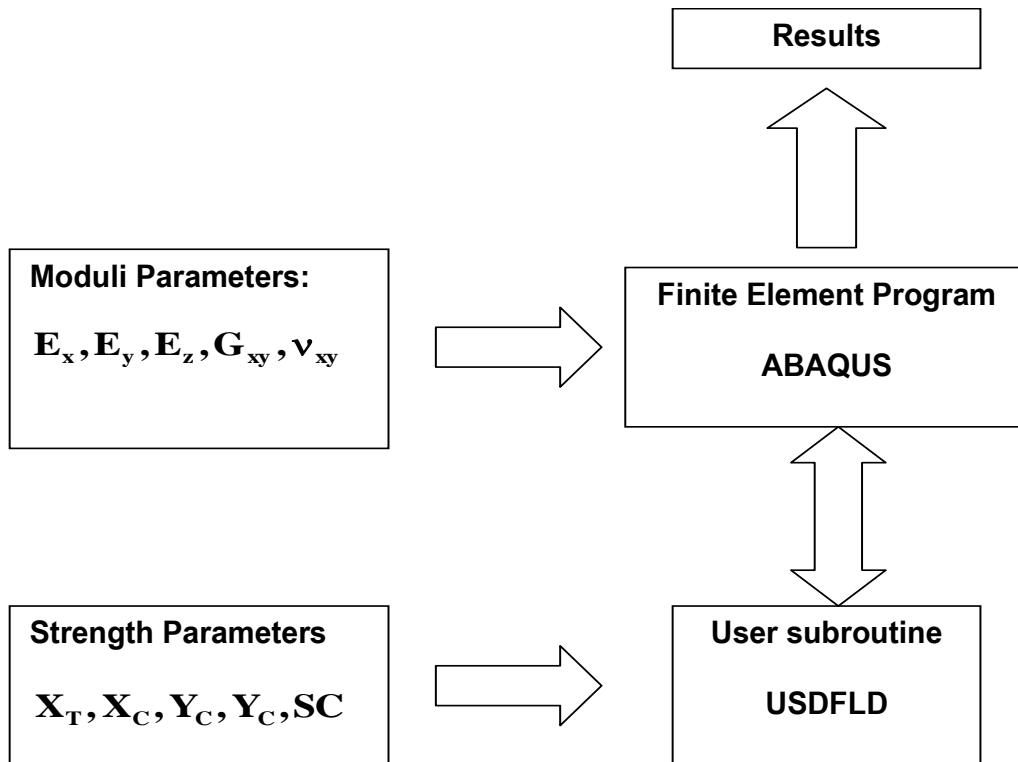


Figure 2.2: Progressive failure analysis.

The full plate is modelled using 20x20 four node shell element S4R of the ABAQUS element library based on first order shear deformation theory. How is shown in figure 2.3 with the subroutine USDFLD it is possible to incorporate in ABAQUS the TSAI-WU criterion:

$$F \equiv \sum_{i=1}^6 F_i \sigma_i + \sum_{i=1}^6 \sum_{j=1}^6 F_{ij} \sigma_i \sigma_j \geq 1 \quad (2.1)$$

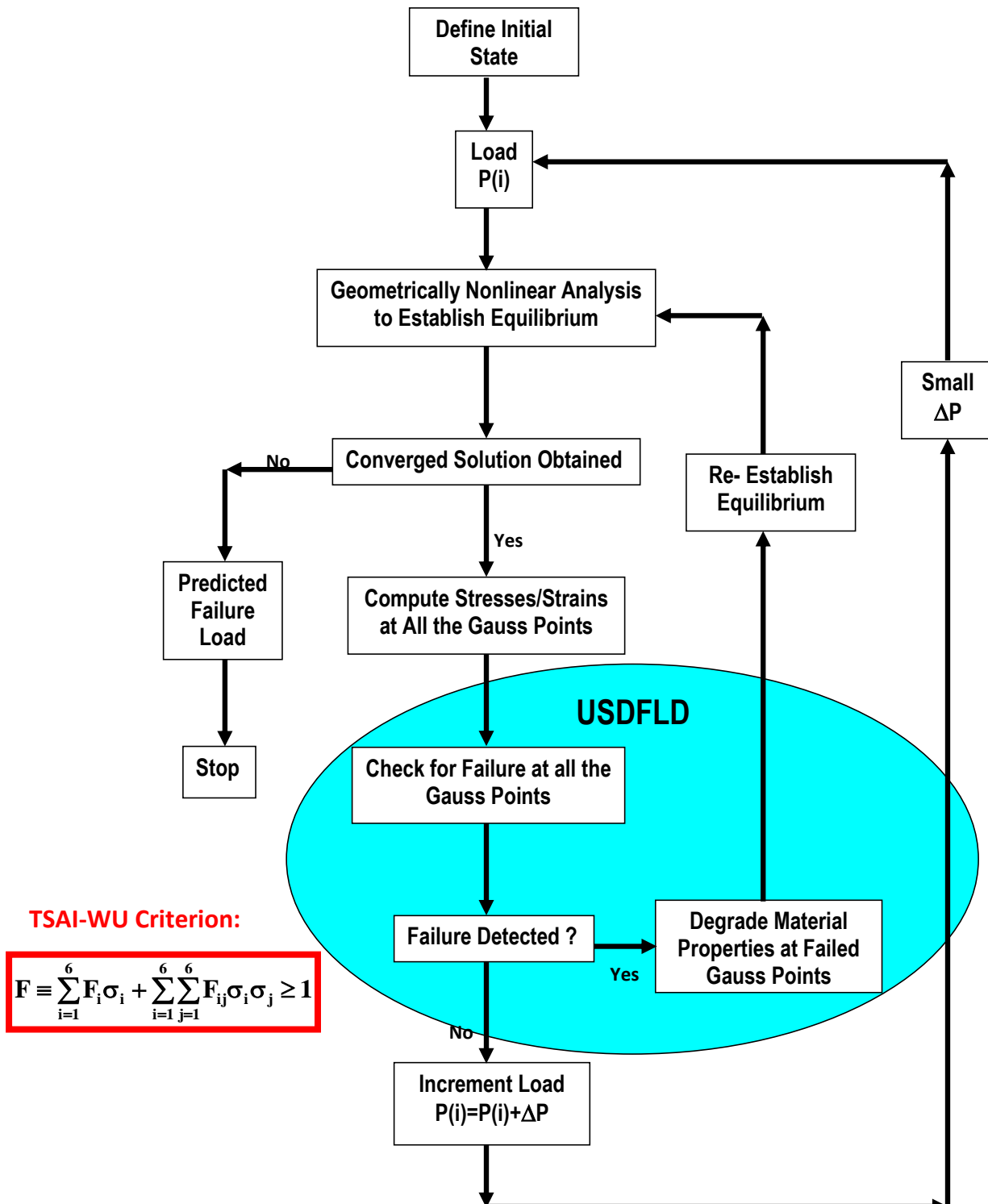


Figure 2.3: Progressive failure analysis.

Where σ_i denotes the stress components referred to the principal material coordinates and the parameters F are function of the lamina normal tension and shear strengths. At each load step, Gauss point stresses are used in the failure criterion. If failure occurred at a Gauss point, a modification of the lamina properties was made at that Gauss point, which results in reduced stiffness of the laminate. To this purpose the following expressions are used to determine the failure mode:

$$\begin{aligned}
 H_1 &= F_1\sigma_1 + F_{11}\sigma_1^2 \\
 H_2 &= F_2\sigma_2 + F_{22}\sigma_2^2 \\
 H_6 &= F_{66}\sigma_6^2
 \end{aligned}
 \tag{2.2}$$

The largest term is selected as the dominant failure mode and the corresponding modulus is reduced to zero. In particular H_1 corresponds to fibre failure, H_2 corresponds to matrix crack and H_6 corresponds to fibre matrix shearing failure. The code implemented in the user subroutine is shown in the flow chart reported in figure 2.4.

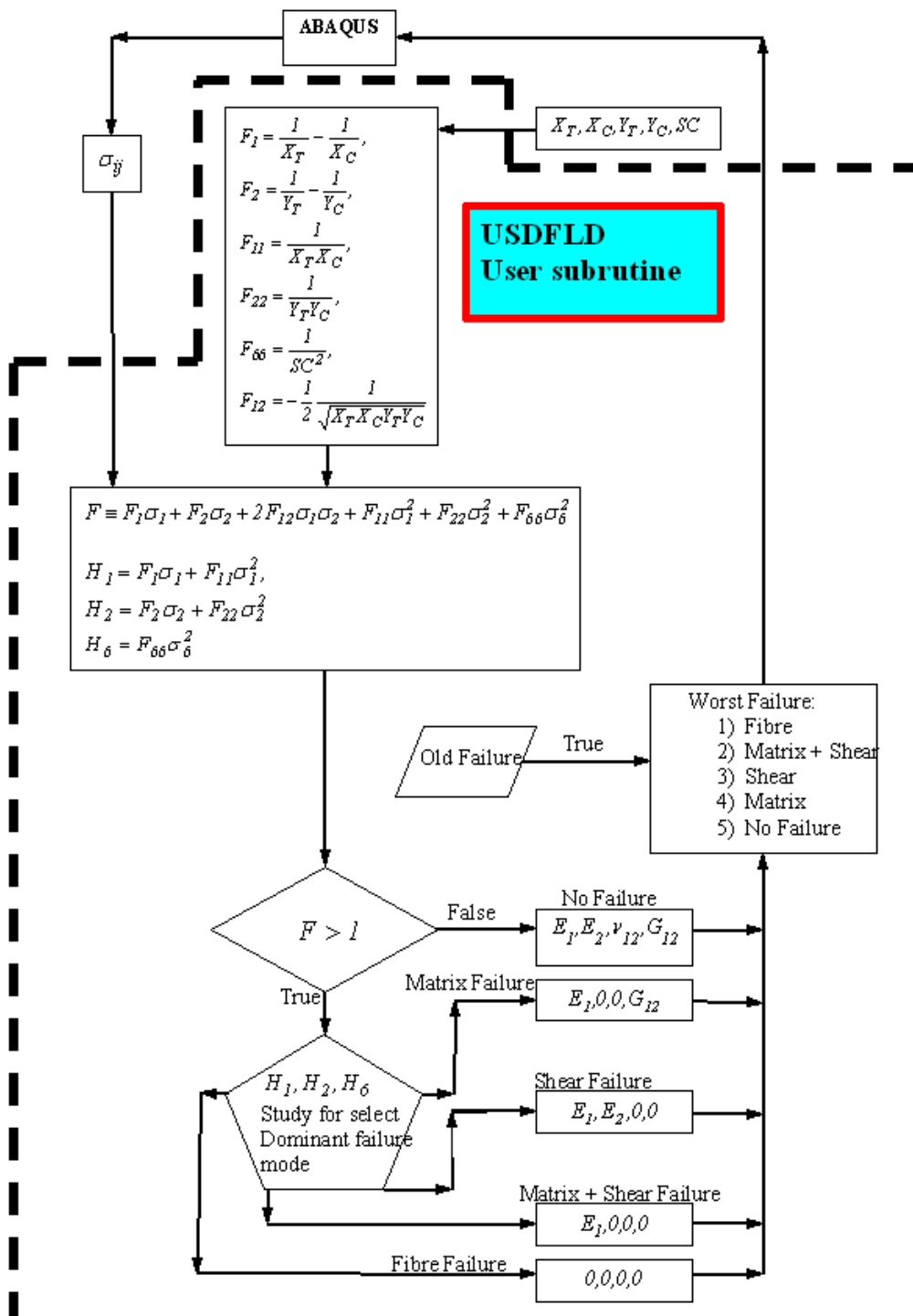
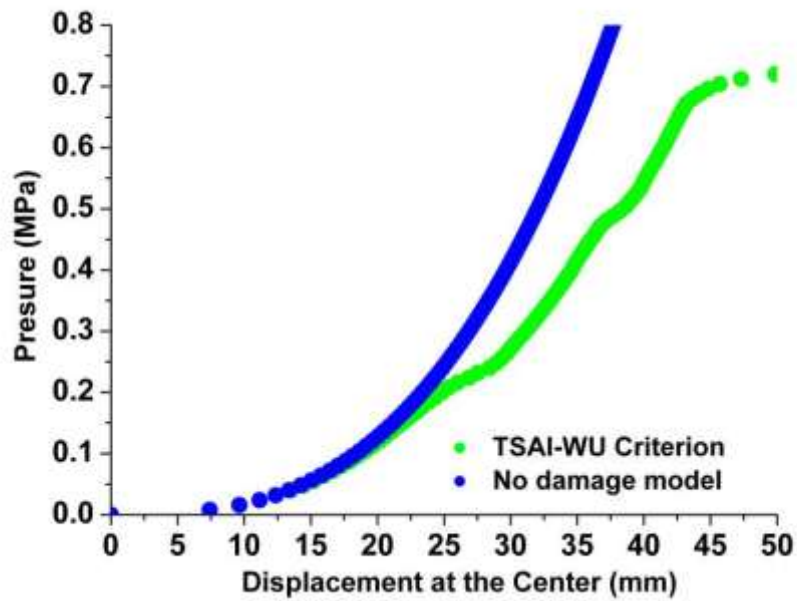


Figure 2.4: Progressive failure analysis.

In figure 2.5 are reported results of the analysis using the standard post processing tools in ABAQUS.



Step: Step-1 Frame: 91

U, U3

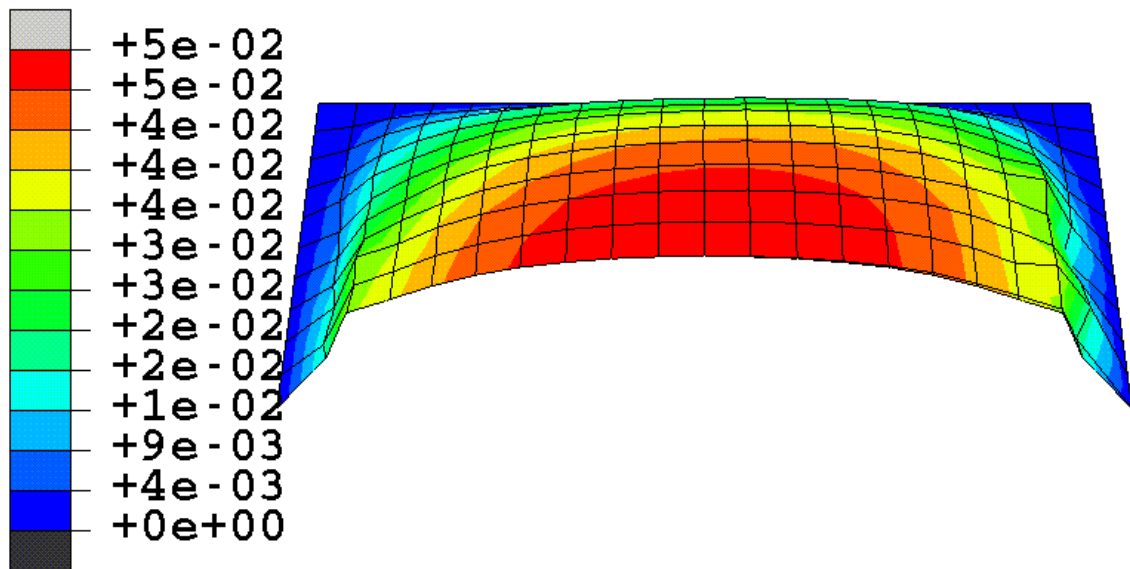


Figure 2.5: Standard ABAQUS representation.

To the top there is the load central deflection graph and to the bottom there is a picture of the deformation of a half part of the plate. But with the standard tools is impossible to visualize where the first ply failure is and how the progression of the damage develops. To answer to these questions we have developed a specific application for post processing visualization of the results.

Used data came from the user subroutine USDFLD and such data have been elaborated through programs written in Fortran 90 whose files of exit have been visualized through the programs of graphic analysis Origin and gOpenMol. Then a specific program was written in Visual Basic that has allowed visualizing all the results of the post elaboration.

The scheme is reported in figure 2.6.

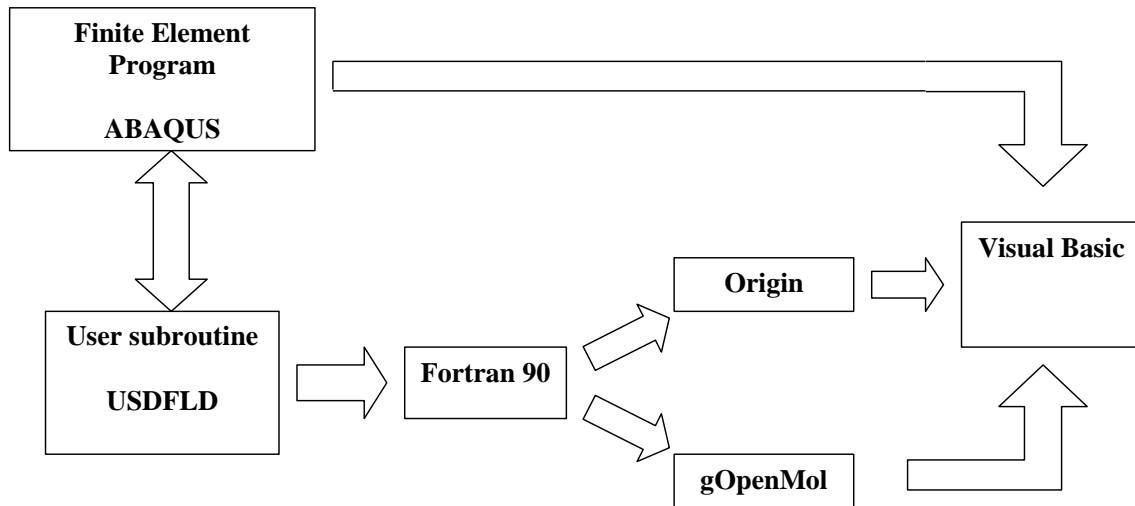


Figure 2.6: Flow chart of the post processing phase.

The graphical user interface used in Visual Basic is shown in figure 2.7.

A pressure increase of 0.008 MPa is used for the analyses and the number of load step is 89.

To the right top there is the load central deflection graph and on its left it is possible to see the move of the deformation of a half part of the plate. To the bottom there are representations of the failure mode with the indication of the percent of the material point with that failure and the number for every play. There is also a graphical representation of the defect positions. Pushing the start button the representation of the time progression of the simulation begins. It is also possible to change the time between two steps. In the graphs horizontal lines show the load that is reached during the progression of the simulation.

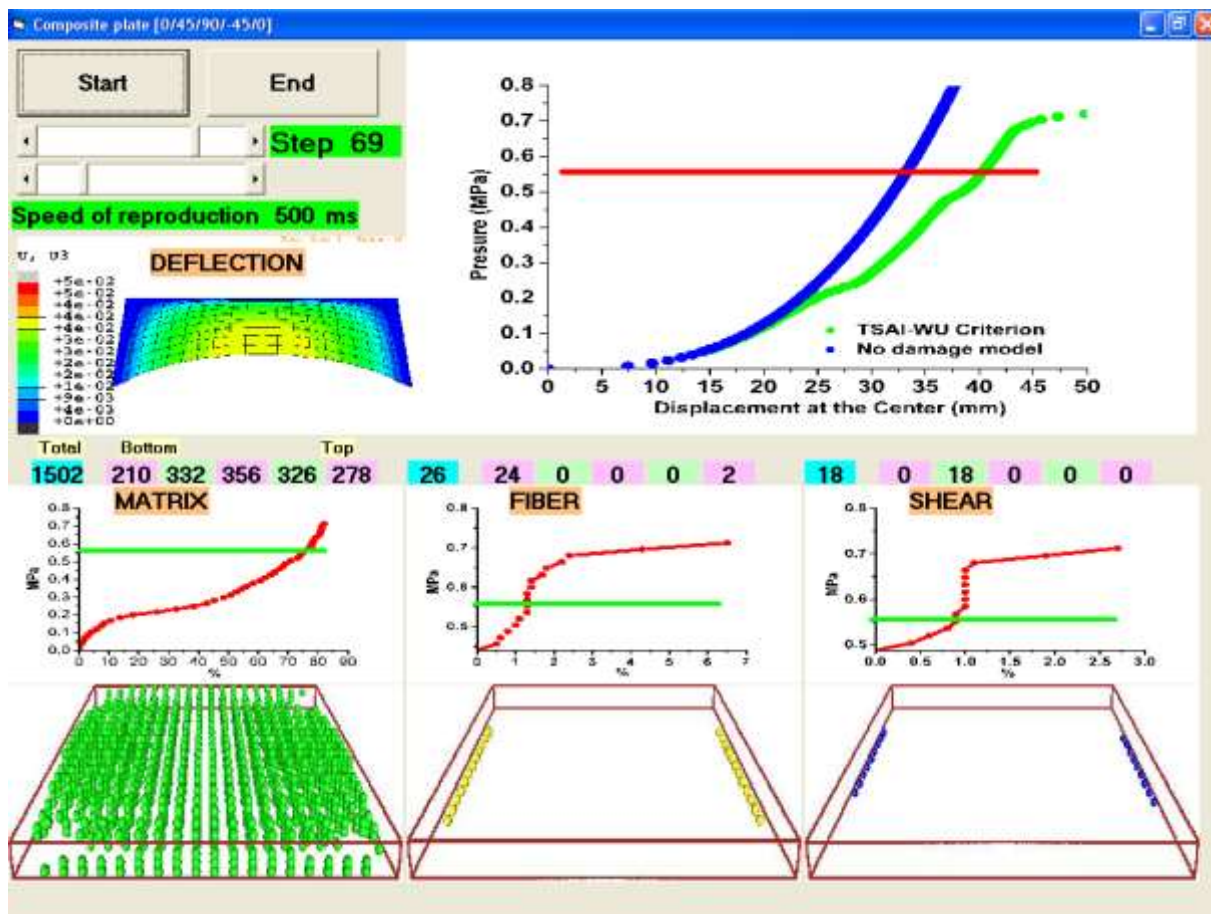


Figure 2.7: Graphical user interface in Visual Basic.

The first ply failure was due to matrix cracking and started from the bottom surface. The drastic change in the central deflection around the pressure of 0.20 MPa is due to the rapid increase of the matrix cracking failure while the change at 0.46 MPa is imputable at the start of the fiber breakage failure. Then the pressure increases bring to a structural collapse due to the fiber breakages spread through the thickness.

In this first approach to the composite material analysis we have developed into one general purpose finite element program a progressive failure methodology for composite plates and we have implemented a specific application to show the type and extent of the damage at a given load, the first ply failure load and the final collapse load.

3. Selection of the environment for the development

The strong limitation in the standard finite element codes, in studying composite materials using multiscale methodology, have led us to seek commercial codes that we could add the necessary micro-scale analysis in a standard finite element software.

The progressive failure method is used on the design of composite materials. In a typical finite element analysis (FEA), failure is assessed at the macro-scale. On the other hand, it is well known that the initiation of damage in composite materials occurs at micro-scale. In commercial there are finite element codes based on computational composite engineering micromechanics that could be a good solution for ours task, therefore develop a multi-scale methodology for composite structural modelling. One of this is GENOA-PFDA (Progressive Failure Dynamic Analysis). Displacement, stress and strain field in a structure are obtained from the finite element solution. The corresponding response fields at the laminate and lamination (macro) scales are calculated using enhanced classical laminated theory. Most of the commercial finite element programs operate strictly at this level. Because the initiation of damage in composite materials occurs at micro-scale (fiber/matrix level), GENOA-PFDA utilized the hierarchical approach illustrated in figure 3.1. The hierarchical modelling reaches down to micro-scale level through the subdivision of unit cells (that in these reports will call RUC representative unit cell) composed of the fiber bundles and surrounding matrix material.

Stress-strain field at the micro-scale are calculated on the basis of macro-scale results, using the computational composite engineering micromechanics. The volume elements of the unit cell are interrogated for possible damage using a set of failure criteria. Once damage at the unit cell level has been detected, GENOA-PFDA degrades the relevant fiber/matrix mechanical properties based on the rules of material behaviour and experience. The accumulation of damage at the micro-level eventually leads to the fracture at the lamina (macro) level. Because damage is tracked at the micro-scale, it is possible to have several types of damage in a particular ply.

The composites and ceramics fail is due to damage growth and accumulation in the fibres, matrix or fiber/matrix interface. Damage growth is driven by increasing load, fatigue cycles, creep or environmental effects. Other affecting damage growth rates are manufacturing flaws, voids and residual stresses, moisture and temperature.

Predicting composite structure failure, durability and life it means predicting composite behaviour at the micro-scale of fiber and matrix, translaminar and interlaminar.

GENOA is an augmentation to FEA adding the necessary micro-scale analysis that gives the possibility of asses the composite failures where they initiate therefore in the fiber, matrix and fiber-matrix interface.

The main components in GENOA are:

- 1) Progressive Failure Analysis (PFA)
- 2) Material Constituent Analyzer (MCA)
- 3) Material Uncertainty Analyzer (MUA)

4) Time Dependent Reliability (TDR)

This code is based on three main functional components:

- 1) Finite Element Software FEA where is used any commercial software package NASTRAN, ABAQUS, ANSYS, etc.
- 2) Full Hierarchical Modelling which goes down to the sub-scale.
- 3) Micro-Mechanics Materials Engineering.

In figure 3.1 it is shown the interaction of GENOA and FEA to perform progressive damage analysis.

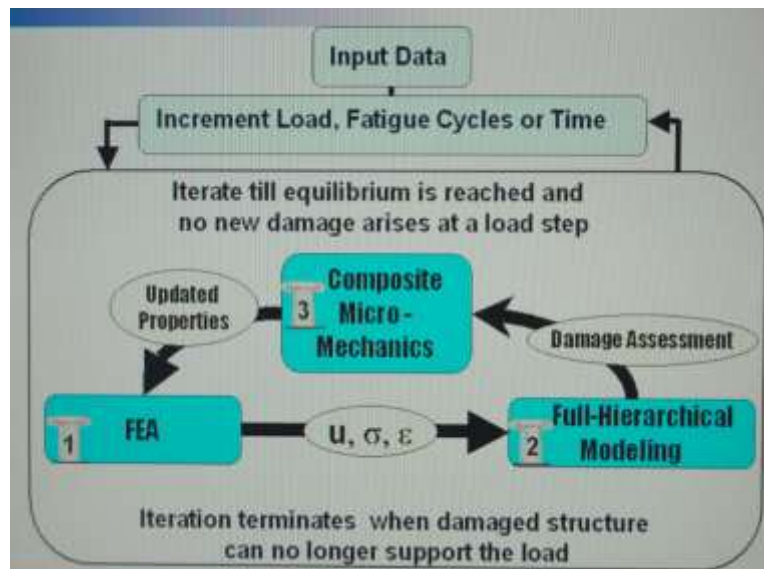


Figure 3.1: Interaction GENOA and FEA.

The FEA solution give displacements (u), stresses (σ) and strains (ε), with these data the Full-Hierarchical Modelling can determine the damage to the level of the fibre and matrix and this information is passed to the Composite Micro-Mechanics which update the stiffness and strength of the fibre and matrix which are the new input for the FEA.

In the figure 3.2 there is a different view of the same process. Above the dot line there is the traditional FEA and lamina theory. Below the line are the capability added by GENOA, there is a unit cell made up of matrix and fiber furthermore, such unit cell is further divided into slice on which is applied the micro-scale analysis.

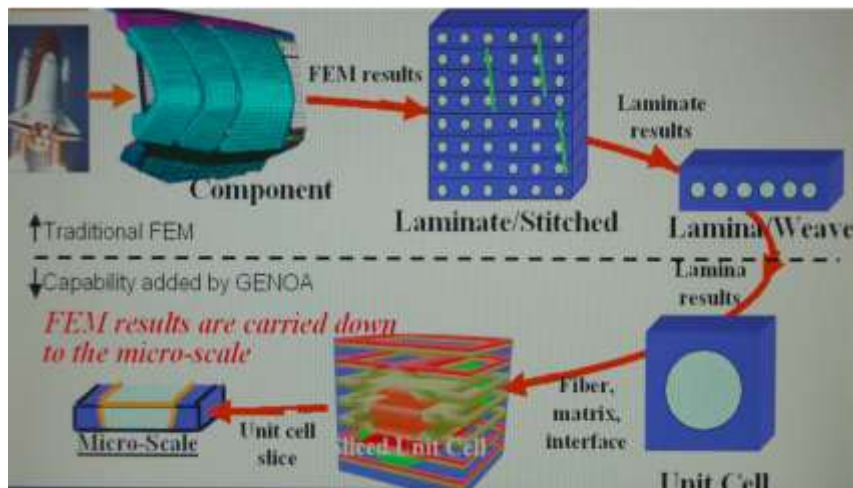


Figure 3.2: Capability added by GENOA to a traditional FEA.

This sub-division is shown in figure 3.3 where at the slide level is employ micro-stress theory that determines where the failures are taking place in the fibre or in the matrix using 16 failure criteria. There are also 6 criteria for assessing the occurrence of delamination between the lamina.

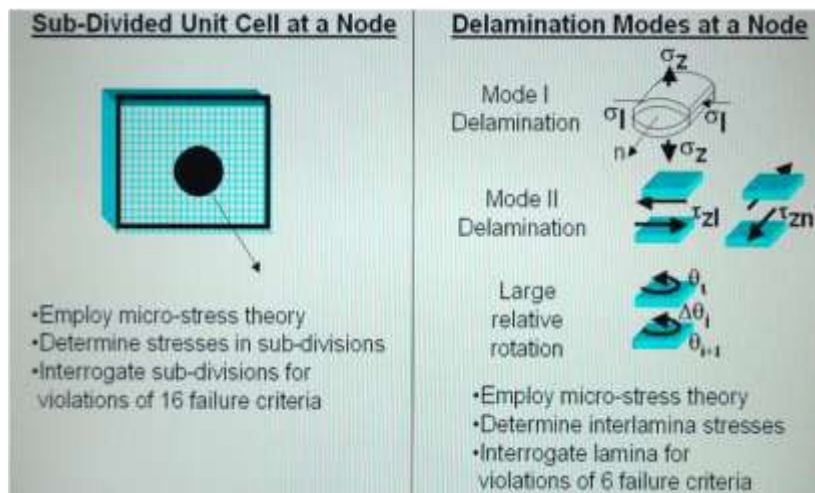


Figure 3.3: Sub-division of the unit cell and mode of delamination.

All the failure criteria are shown in figure 3.4.

Micro-Mechanics Failure Criteria

| | | | |
|---|----------------------------|----|---------------------------------|
| 1 | Longitudinal tension | 9 | Strain invariant failure theory |
| 2 | Longitudinal compression | 10 | Normal compression |
| 3 | Transverse tension | 11 | Custom criteria |
| 4 | Transverse compression | 12 | Normal tension |
| 5 | In-plane shear (+) | 13 | Transverse Normal Shear (+) |
| 6 | In-plane shear (-) | 14 | Transverse Normal Shear (-) |
| 7 | Fiber strain limit | 15 | Longitudinal normal shear (+) |
| 8 | Modified distortion energy | 16 | Longitudinal normal shear (-) |
| | | 17 | Relative rotation criteria |

Unit Cell
Damage
Criteria

Delam.
Criteria

Figure 3.4: Failure criteria.

Close form equations, built at micro-scale level, allow to obtain damage and the consequent reduction of stiffness and strength quickly and then the FEM can run again to assess what happening in the next step of increase of the load. When there is a failure in a particular node (figure 3.5) of the lamina, the code must take into account that the node can no longer bear a load.

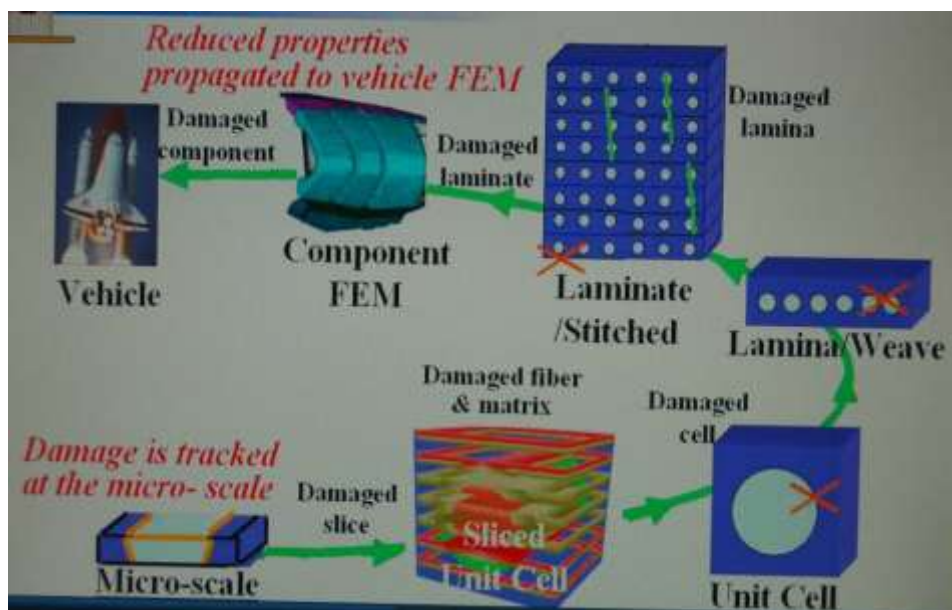


Figure 3.5: Route information of damage from the microscale to the macroscale.

That node is called fractured so the code removes the node. We need to remesh and GENOA automatic remesh (figure 3.6).

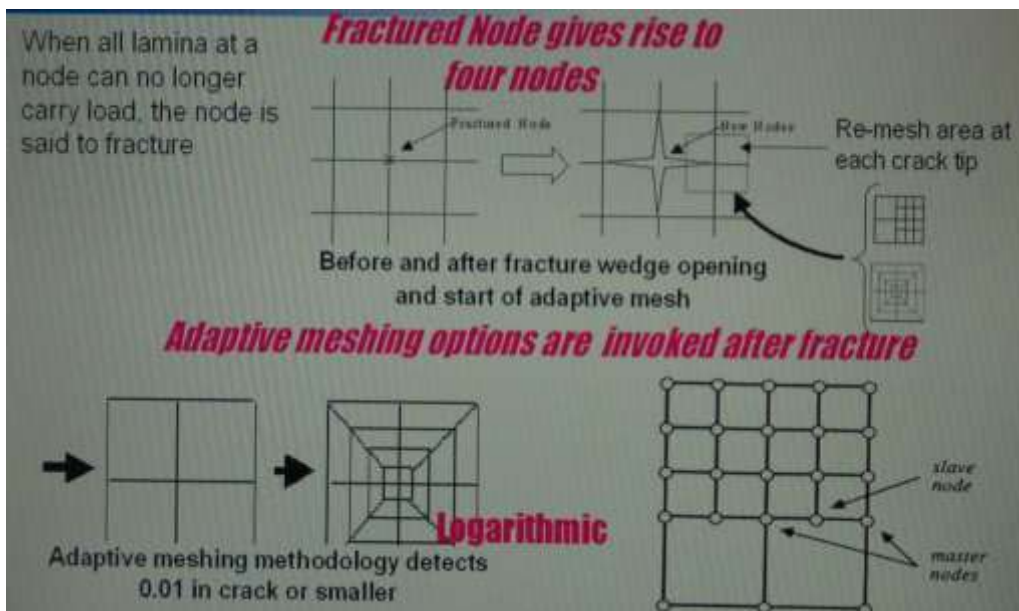


Figure 3.6: Outline of the automatic remesh.

In figure 3.7 is shown the input and the output of GENOA.

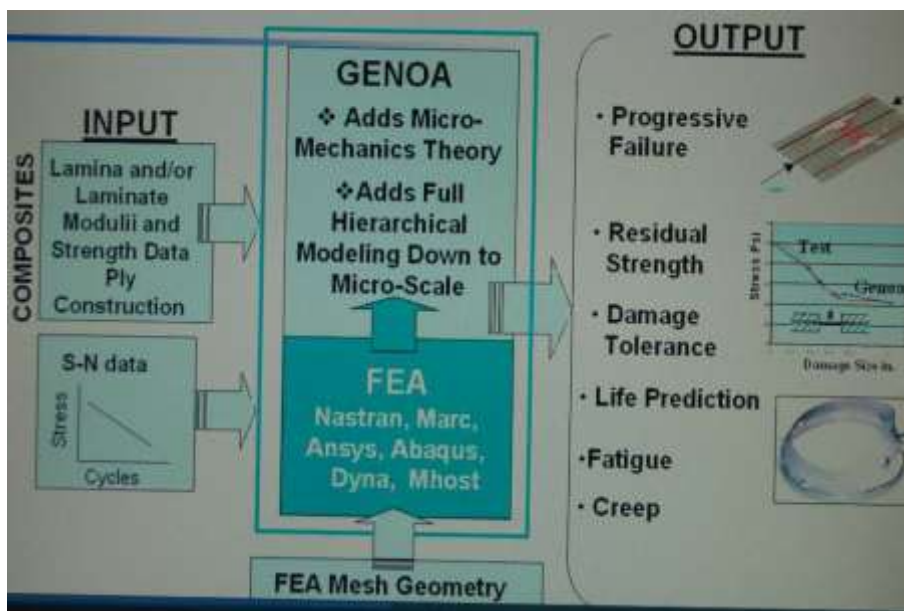


Figure 3.7: Outline of the input and the output in the GENOA code.

The code must be calibrated by knowing the properties of the fibers and matrix. When there is uncertainty on these data it becomes necessary to perform some mechanical tests on specimen of lamina or laminate as shown in figure 3.8.






| Sample Tests on Uniaxial Coupons | | | | |
|---|---|---|--|---|
| Longitudinal Tension | Longitudinal Compression | Transverse Tension | Transverse Compression | Shear |
|  |  |  |  |  |
| ASTM D638, ASTM D3039 | ASTM D695, ASTM D3410 | ASTM D638, ASTM D3039 | ASTM D695, ASTM D3410 | ASTM D3518, ASTM D5379 |

Figure 3.8: Test necessary to calibrate the code.

As it can be seen in figure 3.9 the test results are input to a routine that exists in GENOA, that provides as an output the properties of the fiber and matrix.

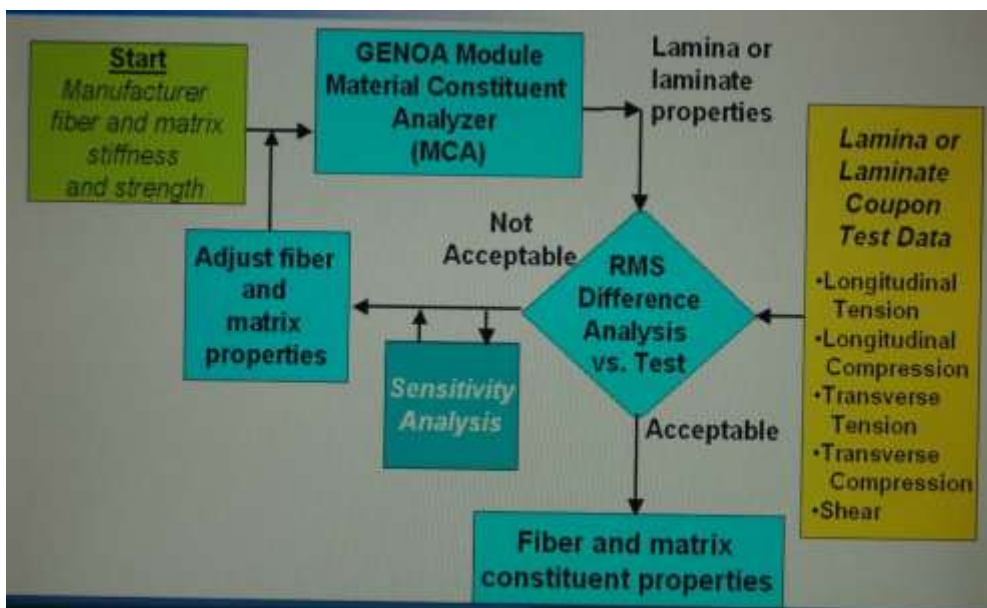


Figure 3.9: Outline for determining the mechanical properties of the fiber and the matrix.

The module named Material Constituent Analyzer (MCA) shown in figure 3.9 calculates lamina (ply) and laminate composite properties knowing the composite architectures and a first estimation of the properties of the fiber and matrix.

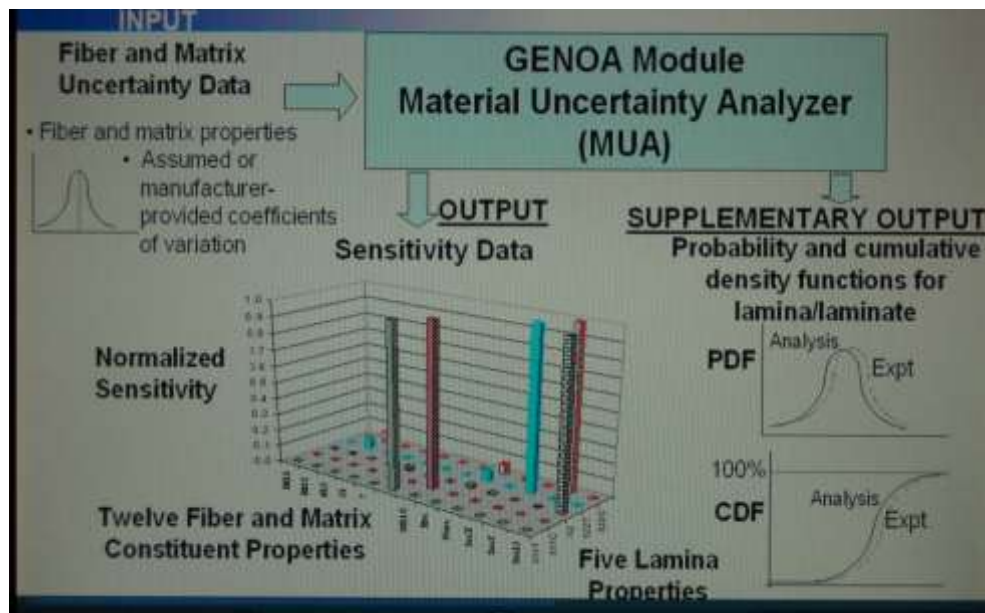


Figure 3.10: Automated sensitivity analysis.

The Sensitivity Analysis, shown in figure 3.9 and in more detail in figure 3.10, is based on the module Material Uncertainty Analyzer (MUA).

This module combines micro-mechanics and probabilistic analysis for study the influence of fundamental primitive variables on the structural response and in particular, on the response sensitivity to constituent material and to other design variables, such as fiber architecture, manufacturing tolerances and defect content.

The output of this module are utilized from the Time Dependent Reliability (TDR) for predict the composite system probability of failure and the sensitivity effects of the material properties, loading conditions and service and manufacturing conditions, so it will be possible targeting design parameter changes, that will be most effective in reducing probability of a given failure mode from occurring, and the probability of failure.

GENOA handles a broad spectrum of composite textile architectures (figure 3.11).

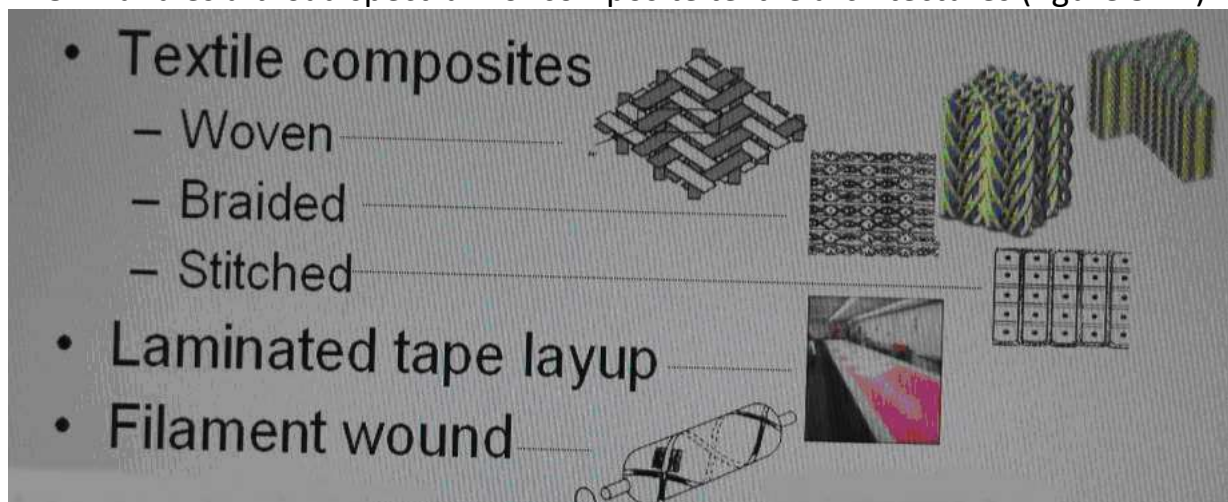


Figure 3.11: Textile architectures covered by GENOA.

4. Constitutive model for a balanced plain weave fabric

The research for a possible commercial environment had shown that in commercially there are finite element codes based on computational composite engineering micromechanics that could be a good solution for our problems. After the research what emerges is that such products are almost totally developed from the NASA ((National Aeronautics and Space Administration) and when commercialized they are characterized by exorbitant costs.

The high cost of the commercial code that could represent a possible environment for development of a model for the structural analysis of ceramic matrix composite material, has brought us to the decision to internally develop a multiscale code based on the commercial software ABAQUS.

This work deals of developing a constitutive model for balanced plain weave fabric (figure 4.1). The micromechanical model was implemented in Fortran [1] programs and user material subroutine for ABAQUS [2], called UMAT, was created out of these programs.

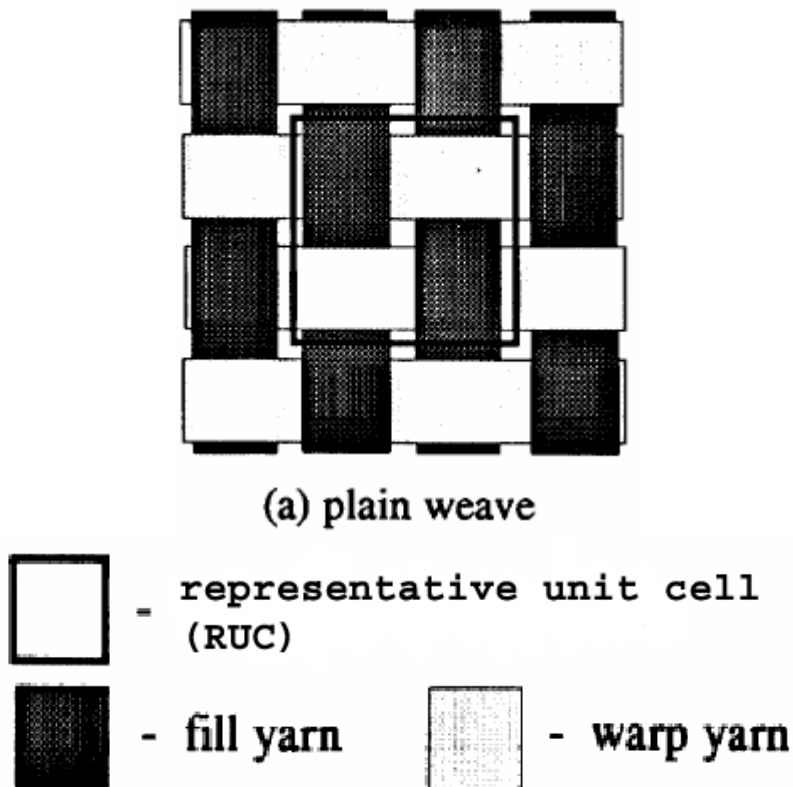


Figure 4.1: Plane weave fabric.

This model starting from geometrical parameter and mechanical parameter of the single constituents (fiber and matrix), determines the effective moduli of the representative unit cell (RUC) shown in figure 4.2 [3].

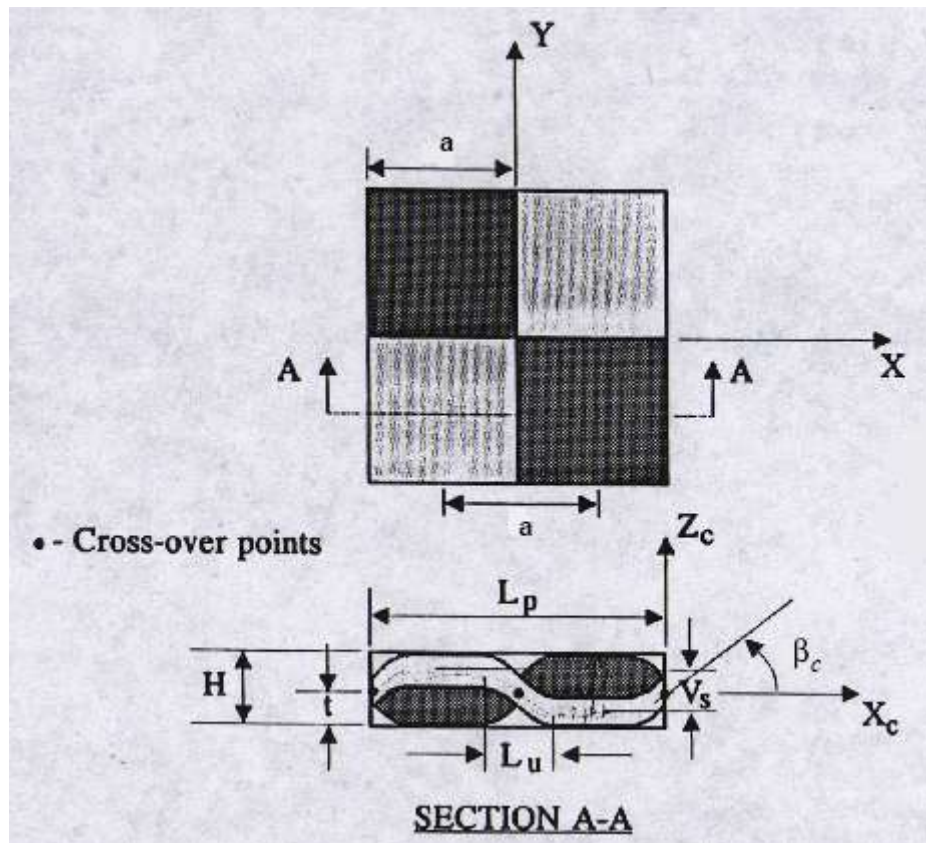


Figure 4.2: Plain weave RUC geometry and notation.

This model was implemented in the structural analysis software system ABAQUS, writing a specific subroutine called UMAT. This UMAT subroutine provides the capability to combine a new material model with the powerful numerical algorithms for structural analysis available in ABAQUS.

The last part of this job was to determine a material failure mechanism theory for balanced plain weave architecture and implement this model in a specific subroutine in the ABAQUS structural analysis software.

The geometric model was developed with the following assumptions:

1. The yarn spacing (quantity a in figure 4.3) for the fill and warp yarns are assumed to be equal.
2. There is no gap between adjacent yarns.
3. The centreline of the yarn path consists of undulation portions and straight portions, with the centreline of undulating portions described by the sine function as drawn in figure 4.4.
4. The cross-section area and the thickness of the yarn normal to its centreline are uniform along the arc-length of the centreline.

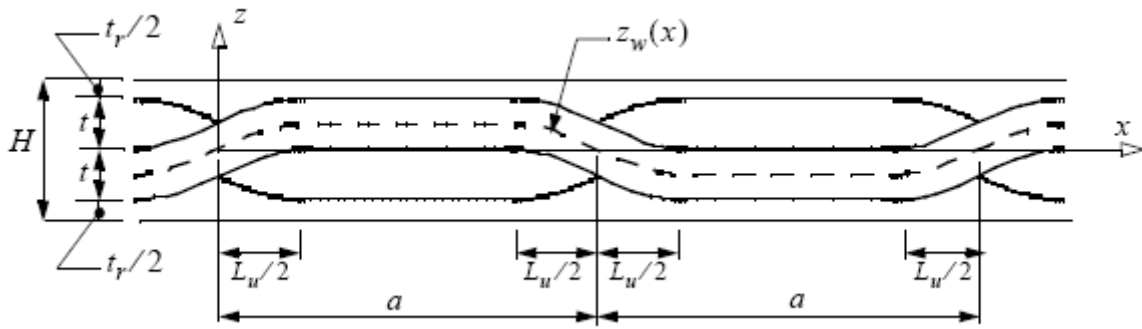


Figure 4.3: Cross section of the RUC along the warp yarn.

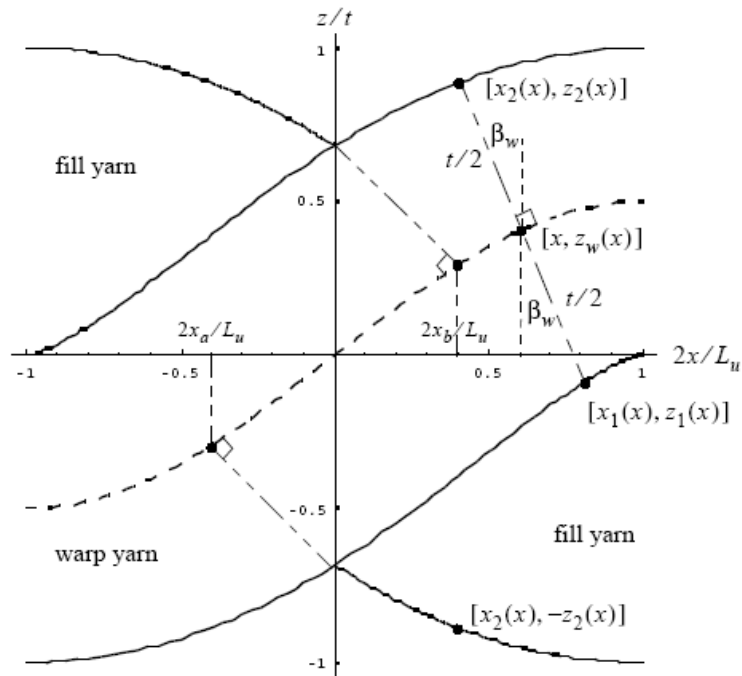


Figure 4.4: Geometry of an undulation region along the warp yarn.

The input parameters for the Fortran subroutine that solve the nonlinear equations describing the geometry of the balanced plane weave architecture are shown in the flow chart in figure 4.5.

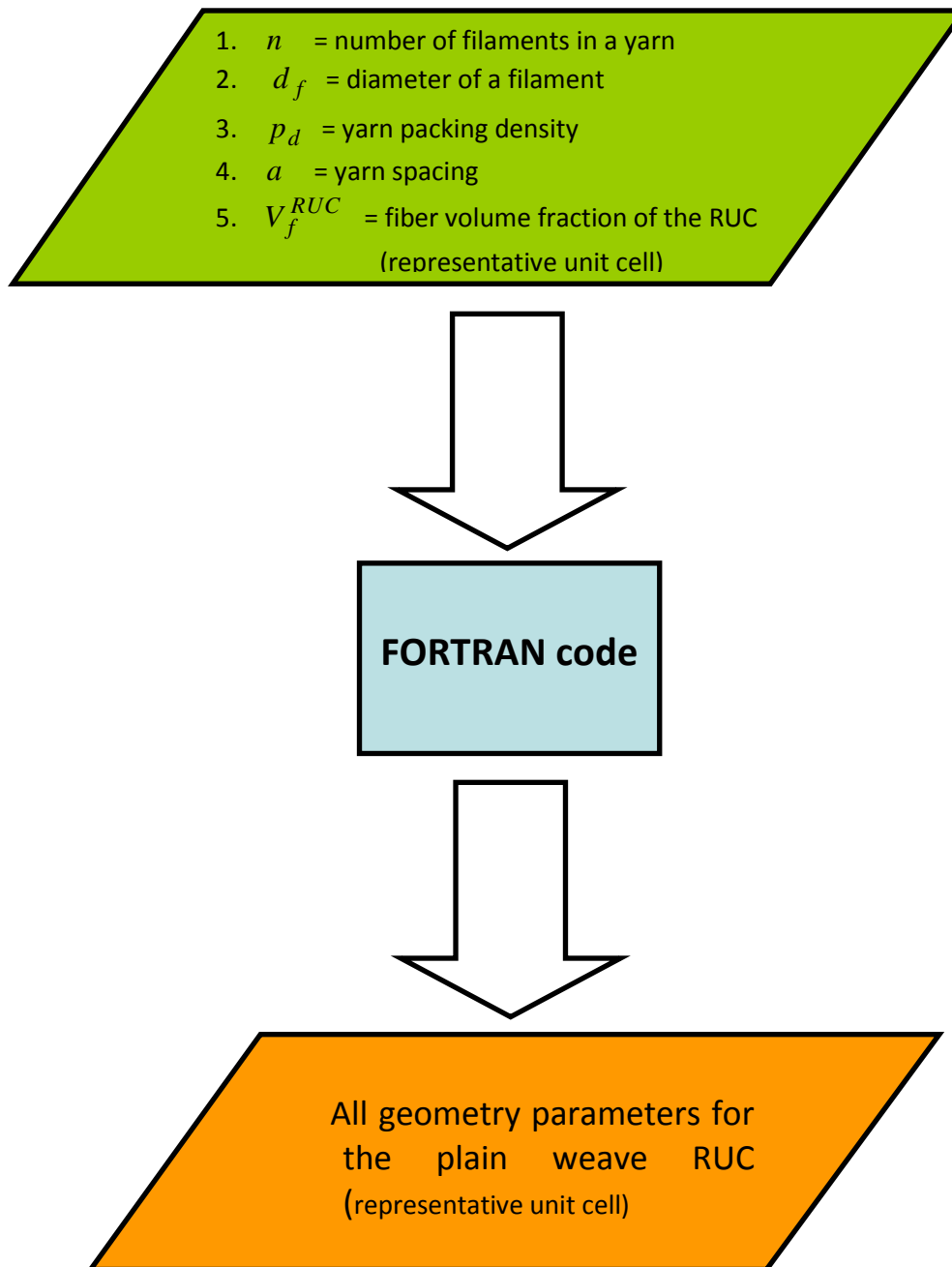


Figure 4.5: Flow chart to resolve the geometry.

The first three parameters describe that the warp and fill yarns contain the same number of filaments n , with all filaments having the same diameter d_f , and the same packing density p_d , that represents the ratio between the whole area of the filaments and the yarn cross section area (figure 4.6).

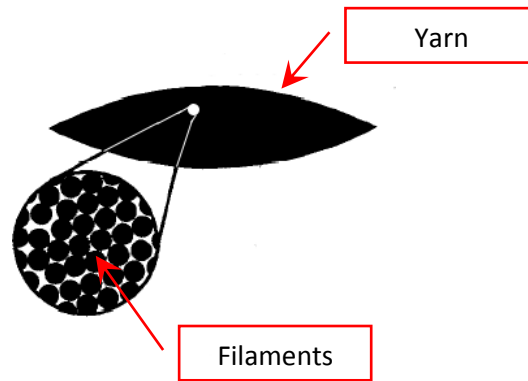
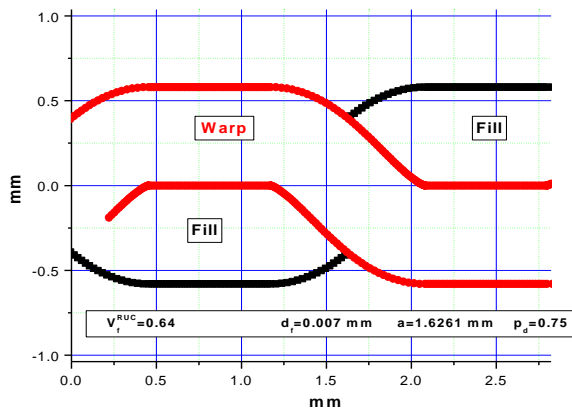


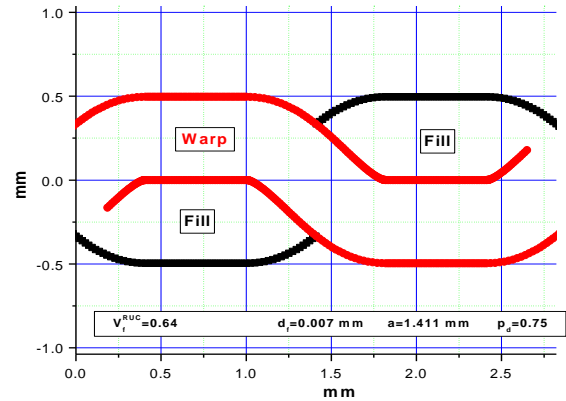
Figure 4.6: The yarn is made with n filaments.

Numerical results of the geometric model, for several values of number of filaments in a yarn, are shown in figure 4.7. In these examples the fibre volume fraction is $V_f^{RUC} = 0.64$, the diameter of a filament is $d_f = 0.007mm$, the yarn spacing is $a = 1.411mm$ and the packing density is $p_d = 0.75$ while the number of filaments is changed from 4000 to 14000. In the figure 4.7 it is possible to see the change in the geometry of the balanced plane weave as a function of the number of the filaments; and it is interesting to note that when this number becomes too large, the codes, to avoid discontinuity in the slope, change in automatic way the value of the yarn spacing that for $n = 14000$ becomes $a = 1.626mm$.

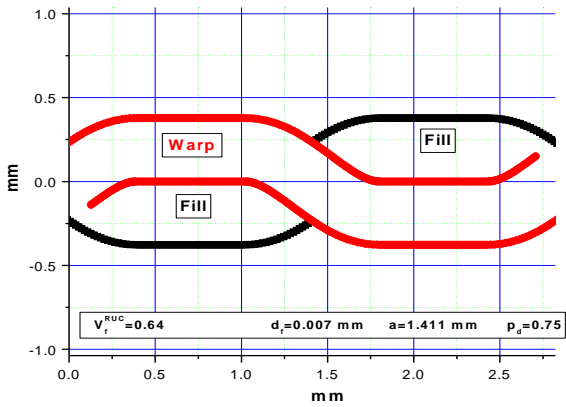
Balanced plain weave number of yarn filaments $n=14000$



Balanced plain weave number of yarn filaments $n=10000$



Balanced plain weave number of yarn filaments $n=8000$



Balanced plain weave number of yarn filaments $n=4000$

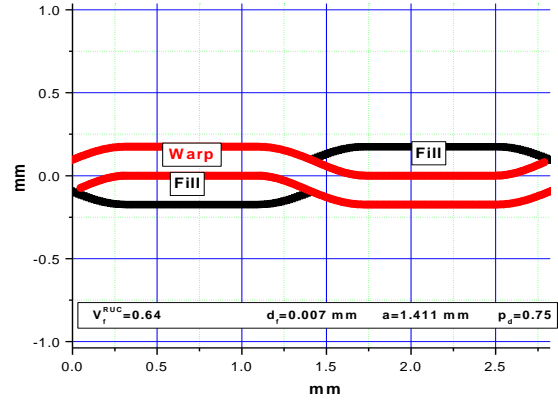


Figure 4.7: Some geometric results.

The calculation of the effective moduli of the representative unit cell (RUC) was developed with the following assumptions:

1. The representative unit cell (RUC) is treated as a spatially oriented fibre composite composed of yarns with transversely isotropic material properties and longitudinal material axes oriented at known angles β and θ how draw in figure 4.8.
2. The RUC (representative unit cell) is composed of three linear elastic phases: two warp yarns, two fill yarns and matrix.
3. Homogenization of the RUC (representative unit cell) to determine its effective moduli is based on iso-strain assumption.

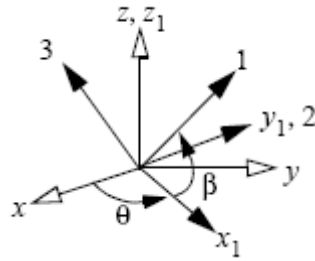


Figure 4.8: Rotations from RUC directions (x, y, z) to yarn directions $(1, 2, 3)$.

The equivalent elasticity matrix for the RUC is defined by:

$$C_{eq} = \frac{1}{V} \left(\int_{V_{warp}} C_{warp} dV + \int_{V_{fill}} C_{fill} dV + \int_{V_{matrix}} C_{matrix} dV \right) \quad (4.1)$$

Where it is evident that the RUC is assumed to be composed of three linear elastic phases: two warp yarns, two fill yarns and resin matrix. In the formula (4.1) V is the volume of the RUC, C_{warp} is the elasticity matrix of the warp, C_{fill} is the elasticity matrix of the fill and C_{matrix} is the elasticity matrix of the matrix.

The (4.1) equation can be re-written in the form:

$$C_{eq} = v_w \cdot C_{eqw} + v_f \cdot C_{eqf} + v_r \cdot C_{eqr} \quad (4.2)$$

Where v_w , v_f and v_r are the volume fractions of the warp yarns, the fill yarns, and the resin and C_{eqw} , C_{eqf} and C_{eqr} are the equivalent elasticity matrices for the warp and fill yarns and for the resin.

The input parameters for the Fortran subroutine that calculated the effective moduli of the RUC for the balanced plane weave architecture are shown in the flow chart in figure 4.9.

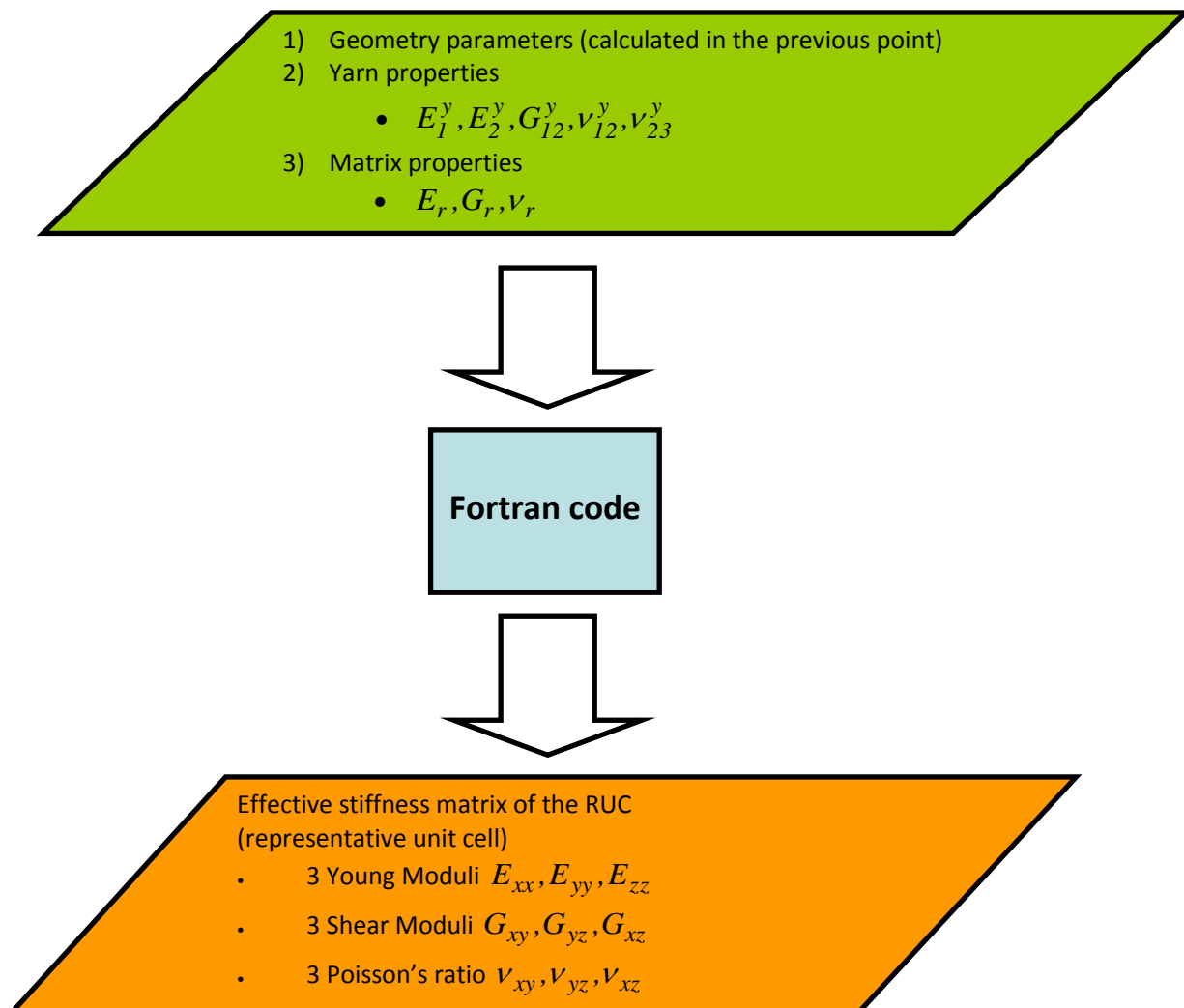


Figure 4.9: Flow chart to calculate the effective moduli of the RUC.

Therefore the calculation of the effective moduli of the RUC needs, knowing the mechanical elastic properties of the warp and fill yarns and the resin mechanical elastic properties, the determination of the following quantities:

- Elasticity matrix for the warp yarn in the global coordinate directions that we identified with $C_I[0, \beta_w(x)]$, where $\theta=0$ and β_w denotes the angle between the x-axis and the tangent to the centreline. This quantity will be function of the direction x. In figure 4.10 are shown some results for the input data reported in table 4.1.
- Elasticity matrix for the fill yarn in the global coordinate directions that we identified with $C_I\left[\frac{\pi}{2}, \beta_f(y)\right]$, where $\theta=\pi/2$ and β_f denotes the angle between the y-axis and the tangent to the centreline. This quantity will be

function of the direction y . In figure 4.11 are shown some results for the input data reported in table 4.1.

- C. Elasticity matrix for the resin in the RUC. The resin elasticity matrix is assumed to be homogeneous and isotropic, so it isn't function of the orientation angles.

Table 4.1:

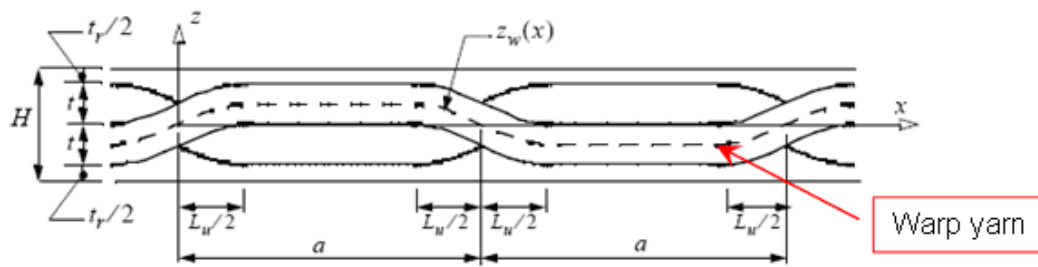
| Geometr y and Mechanical INPUT | | | | | |
|--|-----------------------|-----------------------|--------------------------|------------------------------|------------------------------|
| $n = 10000 \quad a = 1.411 \text{ mm} \quad t = 0.4727 \text{ mm} \quad L_u = 0.7812 \text{ mm}$ | | | | | |
| Material | E_1^y, E_r [GPa] | E_2^y, E_r [GPa] | G_{12}^y, G_r [GPa] | ν_{12}^y, ν_r [GPa] | ν_{23}^y, ν_r [GPa] |
| Yarn | 144.80 | 11.73 | 5.52 | 0.23 | 0.30 |
| Resin | 3.45 | 3.45 | 1.28 | 0.35 | 0.35 |

The elasticity matrix for the yarn that we have identified with C_I is the off-axis matrix that is calculated from the on-axis symmetric six-by-six elasticity matrix C_0 and the transformation of the stress and strain orthogonal six-by-six matrices T_σ and T_ϵ . The relation is defined by:

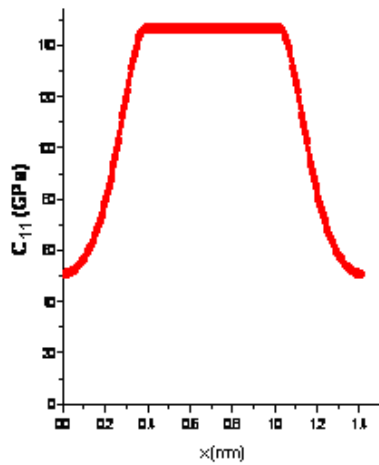
$$C_I(\theta, \beta) = T_\epsilon^T \cdot C_0 \cdot T_\sigma \tag{4.3}$$

For the warp yarn angle $\theta = 0$ and the angle $\beta = \beta_w(x)$. For the fill yarn angle $\theta = \pi / 2$ and the angle $\beta = \beta_f(y)$.

I would like to remember that since the yarns are isotropic in the plane orthogonal to their direction we need five independent material properties.



Element of the elasticity matrix $C_I(0, \beta_w(x))$



Specific element of the elasticity matrix for the warp yarn

Elasticity matrix for warp yarn:

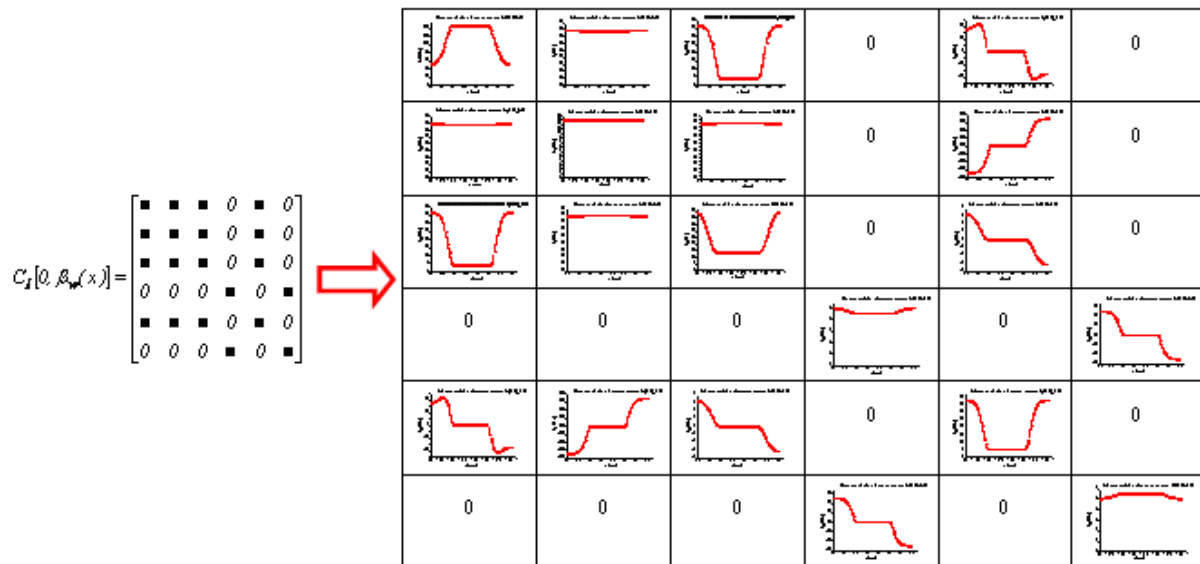


Figure 4.10: Elasticity matrix for the warp yarn.

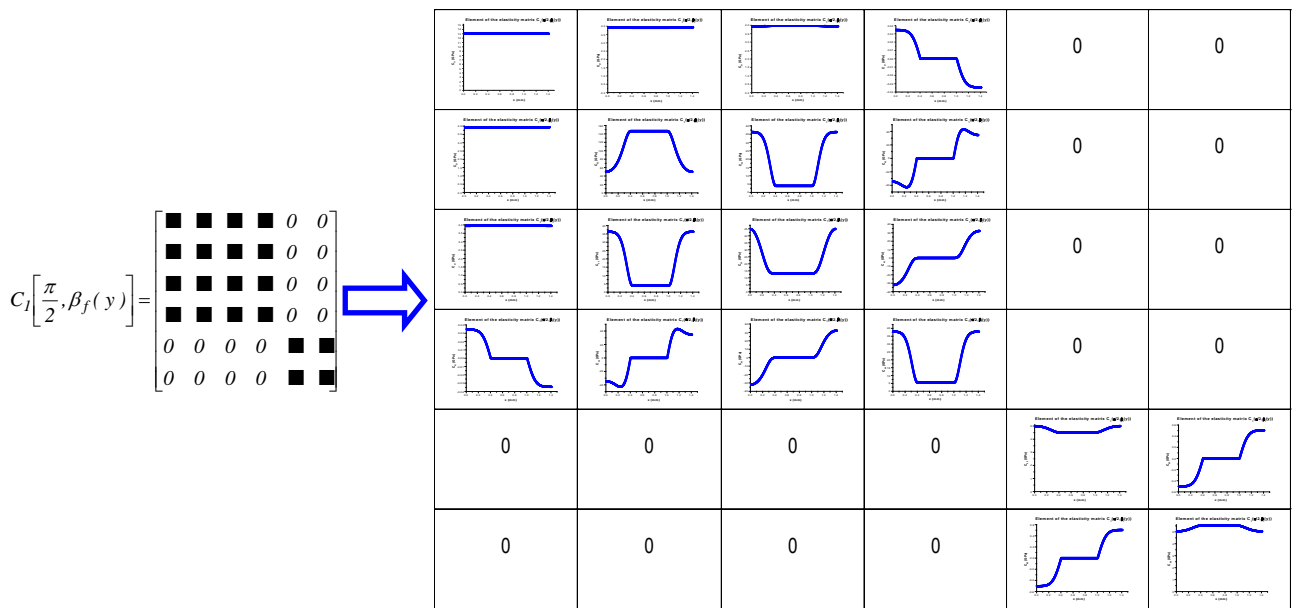
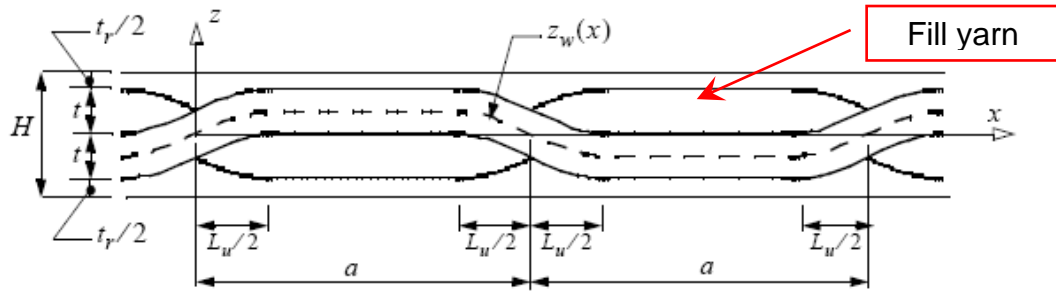


Figure 4.11: Elasticity matrix for the fill yarn

The equivalent elasticity matrices for the warp and fill yarns in equation (4.2) can be expressed as line integrals rather than three dimensional integrals through the following equations:

$$C_{eqw} = \int_0^{2a} function [C_1(0, \beta_w)] \cdot dx = \begin{bmatrix} \blacksquare & \blacksquare & \blacksquare & 0 & 0 & 0 \\ \blacksquare & \blacksquare & \blacksquare & 0 & 0 & 0 \\ \blacksquare & \blacksquare & \blacksquare & 0 & 0 & 0 \\ 0 & 0 & 0 & \blacksquare & 0 & 0 \\ 0 & 0 & 0 & 0 & \blacksquare & 0 \\ 0 & 0 & 0 & 0 & 0 & \blacksquare \end{bmatrix}$$

(4.4)

$$C_{eqf} = \int_0^{2a} function [C_1(\frac{\pi}{2}, \beta_f)] \cdot dy = \begin{bmatrix} \blacksquare & \blacksquare & \blacksquare & 0 & 0 & 0 \\ \blacksquare & \blacksquare & \blacksquare & 0 & 0 & 0 \\ \blacksquare & \blacksquare & \blacksquare & 0 & 0 & 0 \\ 0 & 0 & 0 & \blacksquare & 0 & 0 \\ 0 & 0 & 0 & 0 & \blacksquare & 0 \\ 0 & 0 & 0 & 0 & 0 & \blacksquare \end{bmatrix}$$

Where the elements in the matrices indicated by filled squares denote non-zero values. It can be noted how the material couplings indicated in the equations in figure 4.10 and 4.11 between shear stress and normal strains, and between shear stresses and shear strains, vanish when the integrations in equations (4.4) are performed over the unit cell so the form of the equivalent elasticity matrices for the warp and fill yarns have the same form as for an orthotropic material.

With the input data reported in table 4.1 the results are:

$$C_{eqw} = \int_0^{2a} function [C_1(0, \beta_w)] \cdot dx = \begin{bmatrix} \blacksquare & \blacksquare & \blacksquare & 0 & 0 & 0 \\ \blacksquare & \blacksquare & \blacksquare & 0 & 0 & 0 \\ \blacksquare & \blacksquare & \blacksquare & 0 & 0 & 0 \\ 0 & 0 & 0 & \blacksquare & 0 & 0 \\ 0 & 0 & 0 & 0 & \blacksquare & 0 \\ 0 & 0 & 0 & 0 & 0 & \blacksquare \end{bmatrix} = \begin{bmatrix} 107.17 & 3.90 & 18.41 & 0 & 0 & 0 \\ 3.90 & 12.95 & 3.95 & 0 & 0 & 0 \\ 18.41 & 3.95 & 22.88 & 0 & 0 & 0 \\ 0 & 0 & 0 & 4.68 & 0 & 0 \\ 0 & 0 & 0 & 0 & 20.03 & 0 \\ 0 & 0 & 0 & 0 & 0 & 5.32 \end{bmatrix} \quad (4.5)$$

$$C_{eqf} = \int_0^{2a} function [C_1(\frac{\pi}{2}, \beta_f)] \cdot dy = \begin{bmatrix} \blacksquare & \blacksquare & \blacksquare & 0 & 0 & 0 \\ \blacksquare & \blacksquare & \blacksquare & 0 & 0 & 0 \\ \blacksquare & \blacksquare & \blacksquare & 0 & 0 & 0 \\ 0 & 0 & 0 & \blacksquare & 0 & 0 \\ 0 & 0 & 0 & 0 & \blacksquare & 0 \\ 0 & 0 & 0 & 0 & 0 & \blacksquare \end{bmatrix} = \begin{bmatrix} 12.95 & 3.90 & 3.95 & 0 & 0 & 0 \\ 3.90 & 107.17 & 18.41 & 0 & 0 & 0 \\ 3.95 & 18.41 & 22.88 & 0 & 0 & 0 \\ 0 & 0 & 0 & 20.07 & 0 & 0 \\ 0 & 0 & 0 & 0 & 4.68 & 0 \\ 0 & 0 & 0 & 0 & 0 & 5.32 \end{bmatrix}$$

As we have just said the resin is assumed to be homogeneous and isotropic therefore to build the elasticity matrix we need two independent material properties: the modulus of elasticity E_r and the Poisson's ratio ν_r . With the input data reported in table 4.1 the equivalent elasticity matrix for the resin is:

$$C_{eqr} = \frac{I}{V_{resin}} \int_{V_{resin}} C_{resin} \cdot dV = \begin{bmatrix} \blacksquare & \blacksquare & \blacksquare & 0 & 0 & 0 \\ \blacksquare & \blacksquare & \blacksquare & 0 & 0 & 0 \\ \blacksquare & \blacksquare & \blacksquare & 0 & 0 & 0 \\ 0 & 0 & 0 & \blacksquare & 0 & 0 \\ 0 & 0 & 0 & 0 & \blacksquare & 0 \\ 0 & 0 & 0 & 0 & 0 & \blacksquare \end{bmatrix} = \begin{bmatrix} 5.54 & 2.98 & 2.98 & 0 & 0 & 0 \\ 2.98 & 5.54 & 2.98 & 0 & 0 & 0 \\ 2.98 & 2.98 & 5.54 & 0 & 0 & 0 \\ 0 & 0 & 0 & 1.28 & 0 & 0 \\ 0 & 0 & 0 & 0 & 1.28 & 0 \\ 0 & 0 & 0 & 0 & 0 & 1.28 \end{bmatrix} \quad (4.6)$$

Knowing the equivalent elasticity matrices for the warp and fill yarns and for the resin, it is possible, by applying the equation (4.2), to calculate the equivalent elasticity matrix for the RUC.

$$C_{eq} = v_w \cdot C_{eqw} + v_f \cdot C_{eqf} + v_r \cdot C_{eqr} = \begin{bmatrix} 50.13 & 3.73 & 9.69 & 0 & 0 & 0 \\ 3.73 & 50.13 & 9.69 & 0 & 0 & 0 \\ 9.69 & 9.69 & 19.72 & 0 & 0 & 0 \\ 0 & 0 & 0 & 10.34 & 0 & 0 \\ 0 & 0 & 0 & 0 & 10.34 & 0 \\ 0 & 0 & 0 & 0 & 0 & 4.58 \end{bmatrix} \quad (4.7)$$

From the equivalent elasticity matrix it is possible to calculate the compliance matrix [4]:

$$S_{eq} = C_{eq}^{-1} = \begin{bmatrix} 0.022051 & 0.000497 & -0.011076 & 0 & 0 & 0 \\ 0.000497 & 0.022051 & -0.011076 & 0 & 0 & 0 \\ -0.011076 & -0.011076 & 0.061590 & 0 & 0 & 0 \\ 0 & 0 & 0 & 0.096736 & 0 & 0 \\ 0 & 0 & 0 & 0 & 0.096736 & 0 \\ 0 & 0 & 0 & 0 & 0 & 0.218221 \end{bmatrix} = \begin{bmatrix} \frac{1}{E_{xx}} & -\frac{\nu_{yx}}{E_{yy}} & -\frac{\nu_{zx}}{E_{zz}} & 0 & 0 & 0 \\ -\frac{\nu_{xy}}{E_{xx}} & \frac{1}{E_{yy}} & -\frac{\nu_{zy}}{E_{zz}} & 0 & 0 & 0 \\ -\frac{\nu_{xz}}{E_{xx}} & -\frac{\nu_{yz}}{E_{yy}} & \frac{1}{E_{zz}} & 0 & 0 & 0 \\ 0 & 0 & 0 & \frac{1}{G_{yz}} & 0 & 0 \\ 0 & 0 & 0 & 0 & \frac{1}{G_{xz}} & 0 \\ 0 & 0 & 0 & 0 & 0 & \frac{1}{G_{xy}} \end{bmatrix} \quad (4.8)$$

Now we can calculate the effective material coefficients for the RUC using the relation between the elements of the compliance matrix and the elastic engineering material constants shown in equation (4.8).

In particular for the input data reported in table 4.1 we have gotten the results shown in table (4.2), where the RUC material properties are represented with the

three Young moduli E_{xx} , E_{yy} and E_{zz} the three shear moduli G_{xy} , G_{yz} and G_{xz} the three Poisson's ratio ν_{xy} , ν_{yz} and ν_{xz} .

Table 2.2:

$E_{xx} = 45.35\text{GPa}$; $E_{yy} = 45.35\text{GPa}$; $E_{zz} = 16.24\text{GPa}$; $G_{yz} = 10.34\text{GPa}$; $G_{xz} = 10.34\text{GPa}$; $G_{xy} = 4.58\text{GPa}$
 $\nu_{yz} = 0.50229$; $\nu_{xz} = 0.50229$; $\nu_{xy} = -0.02256$

The geometry module and the module to calculate the effective moduli of the RUC are integrated following the flow chart shown in figure 4.12.

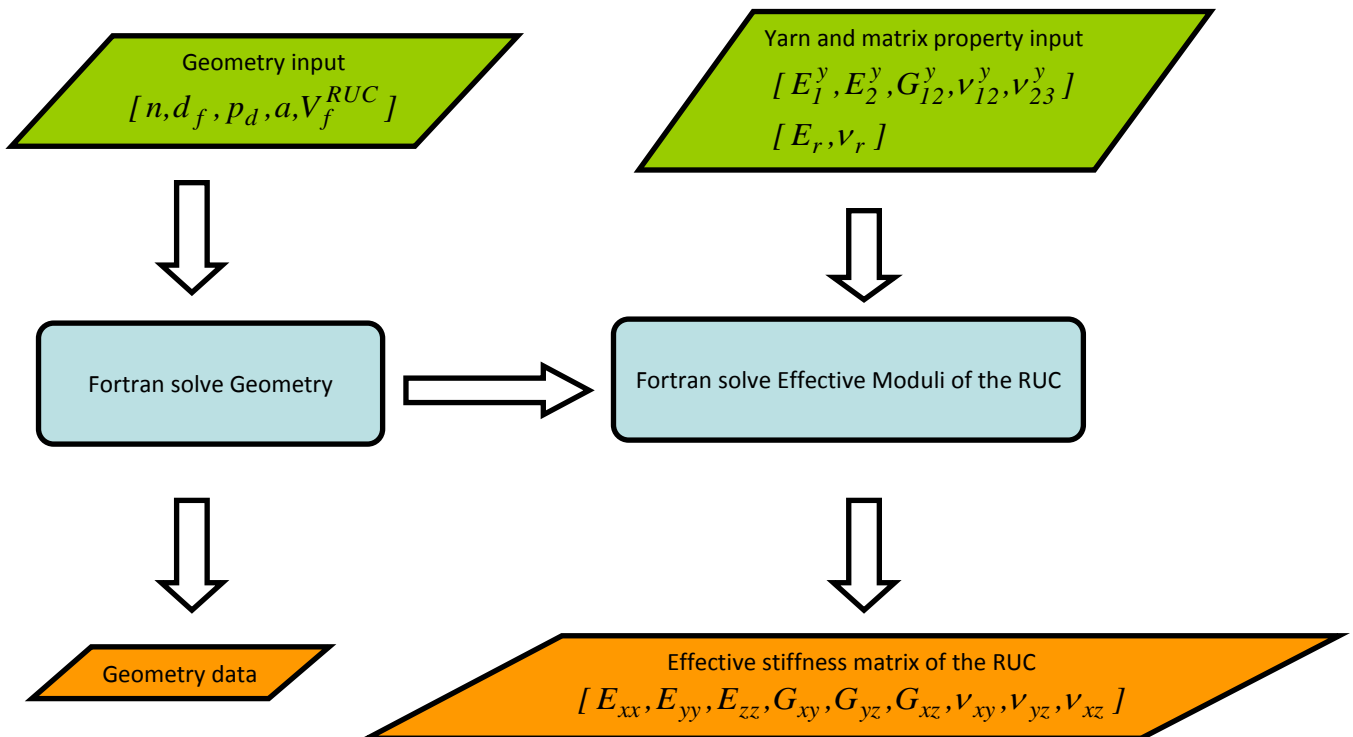


Figure 4.12: Integration of Geometric Modelling and Effective Moduli Calculation.

Numerical results of this integrated model, for several values of number of filaments in a yarn, are shown in figure 4.13. The mechanical properties of the yarns and the resin are that shown in table 4.1. Also the geometry inputs are in table 4.1, but the number of filaments is changed from 2000 to 14000. In the figure 4.13 it is possible to see the change in the geometry and the elastic engineering material constants of the balanced plane weave as function of the number of the filaments. The possibility to change the mechanical properties varying the fabrication architectures enable

advanced design concepts including structural tailoring, multifunctional feature and performance enhancements.

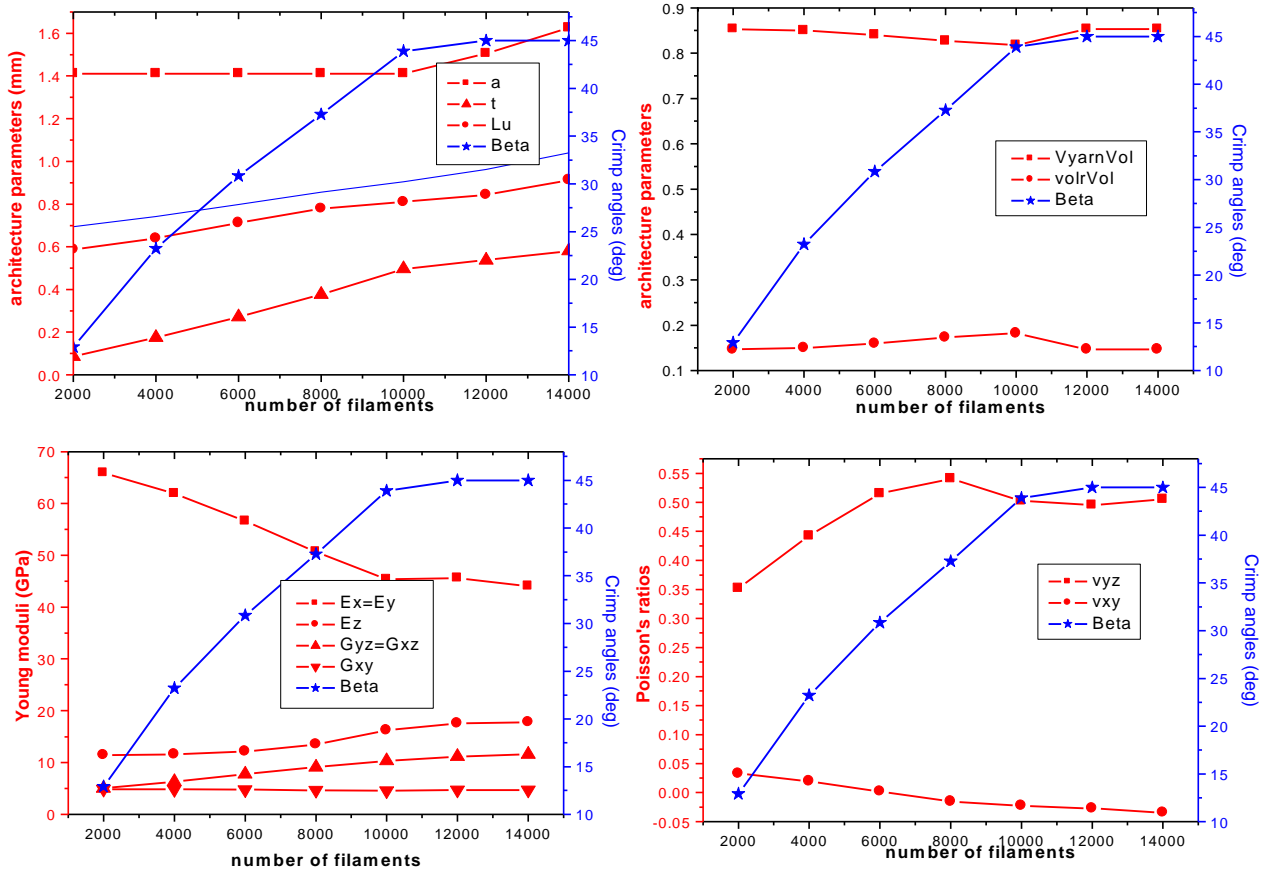


Figure 4.13: Geometric Modelling and Effective Moduli Calculation.

In figure 4.13 the symbols have the following meaning:

$\beta = \beta_c = \text{tangent of the undulation region where } x=0 \text{ (Crimp angle);}$

$t = \text{thickness of the yarn; } a = \text{yarn spacing;}$

$L_u = \text{length of the undulation region; } E_{**} = \text{Young moduli;}$

$G_{**} = \text{Shear moduli; } \nu_{**} = \text{Poisson's ratios;}$

$V_{yarnVol} = V_f^{RUC} = \text{volume fraction of the yarns; } V_{olrVol} = V_r^{RUC} = \text{volume fraction of the resin.}$

Until now we have developed a numerical constitutive model to determine the plain weave effective stiffness matrix. The next step was to implement these constitutive models in the ABAQUS structural analysis software system and to define an incremental finite element approach to progressive failure. Therefore in this last phase we had to determine a material failure mechanism theory for the balanced plain weave architecture.

The prediction of failure at each increment step was obtained by using a quadratic failure criterion, applied to the local strains with stiffness and strength reduction scheme to account for damage within the yarns. In particular we thought to use the Tsai theory [5] to account for progressive degradation of the strengths and stiffnesses of the yarns. The theory does not consider delamination phenomena at the interface between the yarn and the resin system within the RUC.

The Tsai-Wu quadratic criterion in the strain space is:

$$G_{11}\varepsilon_1^2 + 2G_{12}\varepsilon_1\varepsilon_2 + G_{22}\varepsilon_2^2 + G_{66}\varepsilon_6^2 + G_1\varepsilon_1 + G_2\varepsilon_2 = 1 \quad (4.9)$$

Where the parameters G are:

$$G_{11} = F_{11}Q_{11}^2 + 2F_{12}Q_{11}Q_{12} + F_{22}Q_{12}^2$$

$$G_{22} = F_{11}Q_{12}^2 + 2F_{12}Q_{12}Q_{22} + F_{22}Q_{22}^2$$

$$G_{12} = F_{11}Q_{11}Q_{12} + F_{12}(Q_{11}Q_{22} + Q_{12}^2) + F_{22}Q_{12}Q_{22} \quad (4.10)$$

$$G_{66} = F_{66}Q_{66}^2$$

$$G_1 = F_1Q_{11} + F_2Q_{12}$$

$$G_2 = F_1Q_{12} + F_2Q_{22}$$

The strength parameters F are given as function of the material strengths for the yarns. They are: the tensile strength in the yarn direction X_t , the compressive strength in the yarn direction X_c , the tensile strength in the transverse direction Y_t , the compressive strength in the transverse direction Y_c and the in-plane longitudinal shear strength S .

$$\begin{aligned}
 F_{11} &= \frac{I}{X_t X_c} \\
 F_{22} &= \frac{I}{Y_t Y_c} \\
 F_1 &= \frac{I}{X_t} - \frac{I}{X_c} \\
 F_2 &= \frac{I}{Y_t} - \frac{I}{Y_c} \\
 F_{66} &= \frac{I}{S^2} \\
 F_{12} &= \frac{F_{12}^*}{\sqrt{X_t X_c Y_t Y_c}}
 \end{aligned} \tag{4.11}$$

Where $-1 \leq F_{12}^* \leq 1$ and we take the generalized von Mises value $F_{12}^* = -1/2$. The reduced stiffnesses for the yarns along the axis are obtained from the five yarn independent material properties that are the modulus of elasticity along the yarn E_1^y , the modulus of elasticity transversally to the yarn E_2^y , the Poisson ratio $\nu_{12}^y = \nu_{13}^y$, the Poisson ratio ν_{23}^y and the shear modulus G_{12}^y .

$$\begin{aligned}
 Q_{11} &= \frac{E_1^y}{(1 - \nu_{12}^y \nu_{21}^y)} \\
 Q_{22} &= \frac{E_2^y}{(1 - \nu_{12}^y \nu_{21}^y)} \\
 Q_{12} &= \nu_{21}^y Q_{11} = \nu_{12}^y Q_{22} \\
 Q_{66} &= G_{12}^y
 \end{aligned} \tag{4.12}$$

As you can note we assume that the users know the material properties of the yarns. But the code can start the analysis from the properties of the constituents of the yarn therefore filaments and resin. We have used a modified rule of mixtures based on the definition of the stress partitioning parameter that is treated as an empirical constant, so the model needs to have as input two stress partitioning parameters: one for the transverse Young's modulus P_y^* and one for the longitudinal shear modulus P_s^* . The inputs to the micromechanic module are the filament

properties that is assumed to be transversely isotropic so we need five independent parameters: the modulus of elasticity along the filament E_1^f , the modulus of elasticity transversally to the filament E_2^f , the Poisson ratio $\nu_{12}^f = \nu_{13}^f$, the Poisson ratio ν_{23}^f and the shear modulus G_{12}^f . We also need to know the properties of the resin into the yarn that is assumed to be isotropic so there are two independent parameters the modulus of elasticity E_r^y and the Poisson's ratio ν_r^y . The relations are:

$$\begin{aligned}
 E_1^y &= V_f^y \cdot E_1^f + (1 - V_f^y) \cdot E_r^y \\
 \nu_{12}^y &= V_f^y \cdot \nu_{12}^f + (1 - V_f^y) \cdot \nu_r^y \\
 \frac{1}{E_2^y} &= \frac{1}{1 + P_y^*} \cdot \left(\frac{1}{E_2^f} + \frac{P_y^*}{E_r^y} \right) \\
 \frac{1}{G_{12}^y} &= \frac{1}{1 + P_s^*} \cdot \left(\frac{1}{G_{12}^f} + \frac{P_s^*}{G_r^y} \right) \\
 \frac{1}{G_{23}^y} &= \frac{1}{1 + P_s^*} \cdot \left(\frac{1}{G_{23}^f} + \frac{P_s^*}{G_r^y} \right)
 \end{aligned}
 \tag{4.13}$$

Where:

$$\begin{aligned}
 G_r^y &= \frac{E_r^y}{2 \cdot (1 + \nu_r^y)} \\
 G_{23}^y &= \frac{E_2^y}{2 \cdot (1 + \nu_{23}^y)}
 \end{aligned}
 \tag{4.14}$$

Tsai developed a method to account for degradation of lamina strength and stiffness that we can use for the yarn. This model is based on the sign of the local (on-axis) transverse normal strain to determine if there is matrix or filament failure in the yarn.

If the transverse yarn strain is positive, and there is no prior failure to this yarn, the event is assumed to be a matrix failure inside the yarn. Matrix stiffness and transverse strength are reduced but filament stiffness is retained.

If the transverse yarn strain is negative, or a prior failure has occurred in the yarn, the event is assumed to be a filament failure inside the yarn. This time is used an alternate material degradation model which also reduces the axial stiffness.

The stiffness and strength parameters that are modified in case of damage are: the modulus of elasticity along the yarn E_1^y , the modulus of elasticity transversally to the yarn E_2^y , the Poisson ratio ν_{12}^y , the shear modulus G_{12}^y , the compressive strength in the yarn direction X_c and the parameter F_{12}^* that we can write in a row form:

$$\left[E_1^y \quad E_2^y \quad \nu_{12}^y \quad G_{12}^y \quad X_c \quad F_{12}^* \right] \quad (4.15)$$

If either matrix or filament failure is detected within a yarn, degradation of the local effective yarn stiffnesses and material strengths is obtained by multiplying the yarn material data subject to be modified, equation (4.15), by the following associated column factors:

$$D_m = \begin{bmatrix} 1 \\ \frac{E_2^{ydm}}{E_2^y} \\ E_m^* \\ \frac{G_{12}^{ydm}}{G_{12}^y} \\ \left(\frac{G_{12}^{ydm}}{G_{12}^y} \right)^{n^*} \\ E_m^* \end{bmatrix} \quad (4.16)$$

$$D_f = \begin{bmatrix} E_f^* \\ \frac{E_2^{ydf}}{E_2^y} \\ E_f^* \\ \frac{G_{12}^{ydf}}{G_{12}^y} \\ \left(\frac{G_{12}^{ydf}}{G_{12}^y} \right)^{n^*} \\ E_f^* \end{bmatrix}$$

Constants E_m^* and E_f^* are, respectively, the matrix and filament degradation factors while n^* is a constant that governs the reduction in axial compression strength X_c . The quantities E_2^{ydm} and E_2^{ydf} are, respectively, the degraded modulus of transverse elasticity to the yarn due to matrix and filament damage:

$$\frac{1}{E_2^{ydm}} = \frac{1}{1 + P_y^*} \cdot \left(\frac{1}{E_2^f} + \frac{P_y^*}{E_m^* \cdot E_r^y} \right) \quad (4.17)$$

$$\frac{1}{E_2^{ydf}} = \frac{1}{1 + P_y^*} \cdot \left(\frac{1}{E_2^f} + \frac{P_y^*}{E_f^* \cdot E_r^y} \right)$$

The quantities G_{12}^{ydm} and G_{12}^{ydf} are, respectively, the degraded shear modulus to the yarn due to matrix and filament damage:

$$\frac{1}{G_{12}^{ydm}} = \frac{1}{1 + P_s^*} \cdot \left(\frac{1}{G_{12}^f} + \frac{P_s^*}{E_m^* \cdot G_r^y} \right) \quad (4.18)$$

$$\frac{1}{G_{12}^{ydf}} = \frac{1}{1 + P_s^*} \cdot \left(\frac{1}{G_{12}^f} + \frac{P_s^*}{E_f^* \cdot G_r^y} \right)$$

In a RUC we have two warp yarns and two fill yarns. The matrix failure can precede a filament failure. Filament failure can occur once for yarn and a second indication of filament failure is interpreted as ultimate failure and the strength and stiffness are not degraded further. In figure 4.14 is shown the flow chart of the progressive failure analysis algorithm.

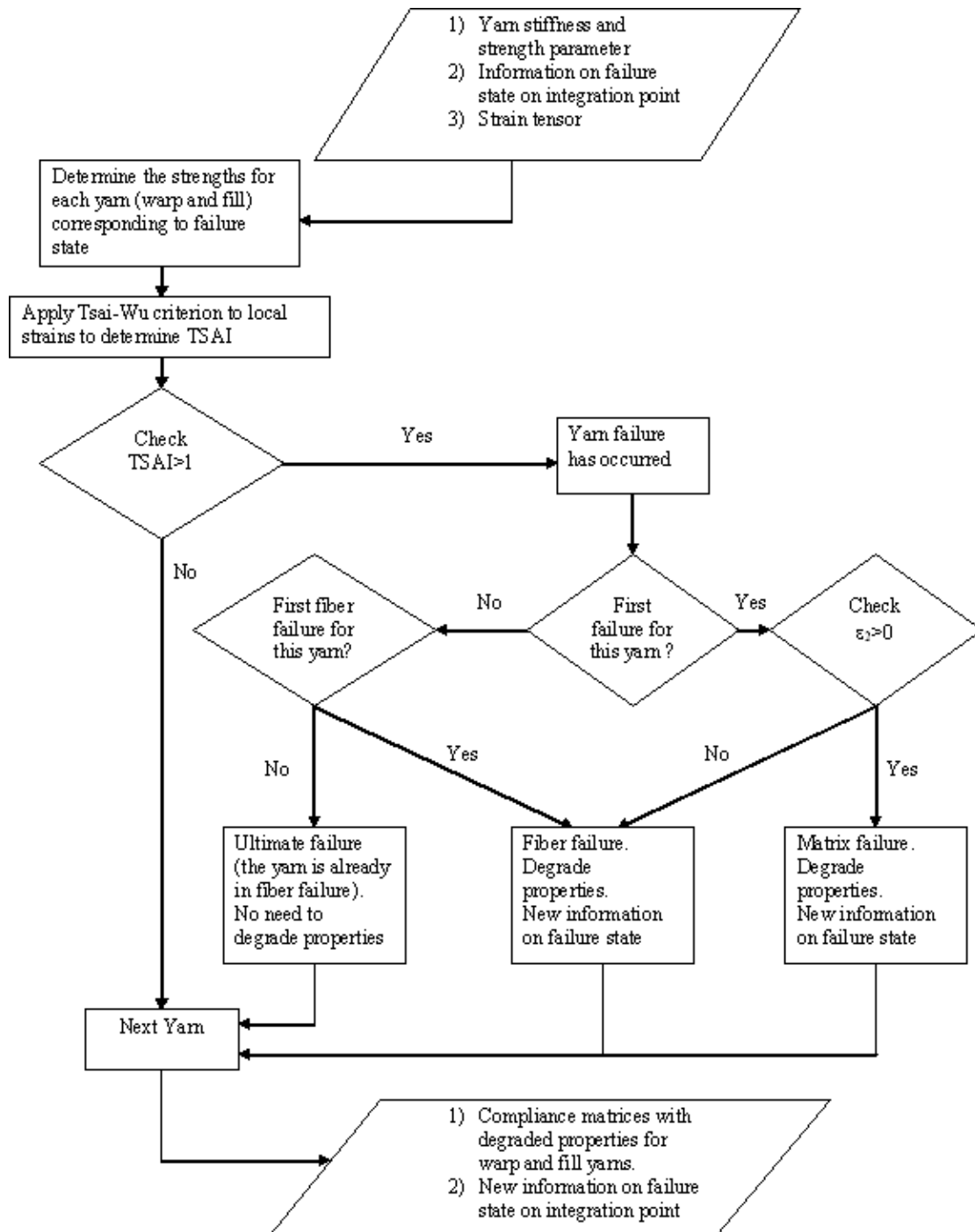


Figure 4.14: Flow chart of the progressive failure analysis algorithm.

We have discretized the warp and fill yarns into slices and for every slice we have computed the Tsai-Wu criterion (figure 4.15).

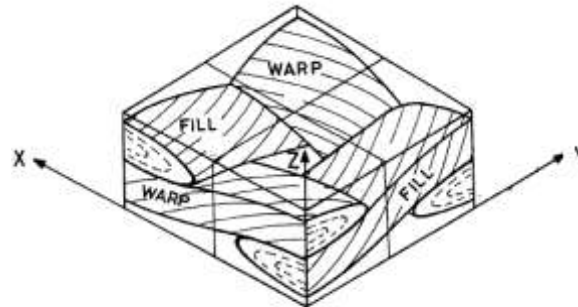


Figure 4.15: Sketch of a part of the RUC subject to discretization.

The yarns in the RCU can be either in one of the four failure states: (1) No failure; (2) Matrix failure; (3) Single filament failure; (4) Matrix failure followed by filament failure. The information on the warp and fill yarns failure states are contained in a specific array in the ABAQUS environment. The name is STATEV(NSTATV) and it contains the solution-dependent state variables; the values can be updated in the user subroutine. The first row corresponds to the warp yarn and the second row to the fill yarn. Therefore the array STATEV can take four different integer values related to four failure states. NSTATV is the number of solution dependent state variables that are associated with this material and they are defined in the *DEPVAR ABAQUS option.

The geometric model, the effective moduli calculation and the material failure model for a balanced plain weave fabric are been included within ABAQUS using the user subroutine UMAT that allows the definition of a particular material's mechanical behaviour. This subroutine is called, in the ABAQUS analysis process, at all material calculation points of elements for which the material definition includes the *USER MATERIAL option.

In figure 4.16 is shown the flow chart of the implementation of the code in ABAQUS. A basic concept in ABAQUS is the division of the problem history into steps. Within each step, a number of solution increments may be performed depending on the type of analysis for that solution step. The time increment variable is used to scale the applied loads and displacements.

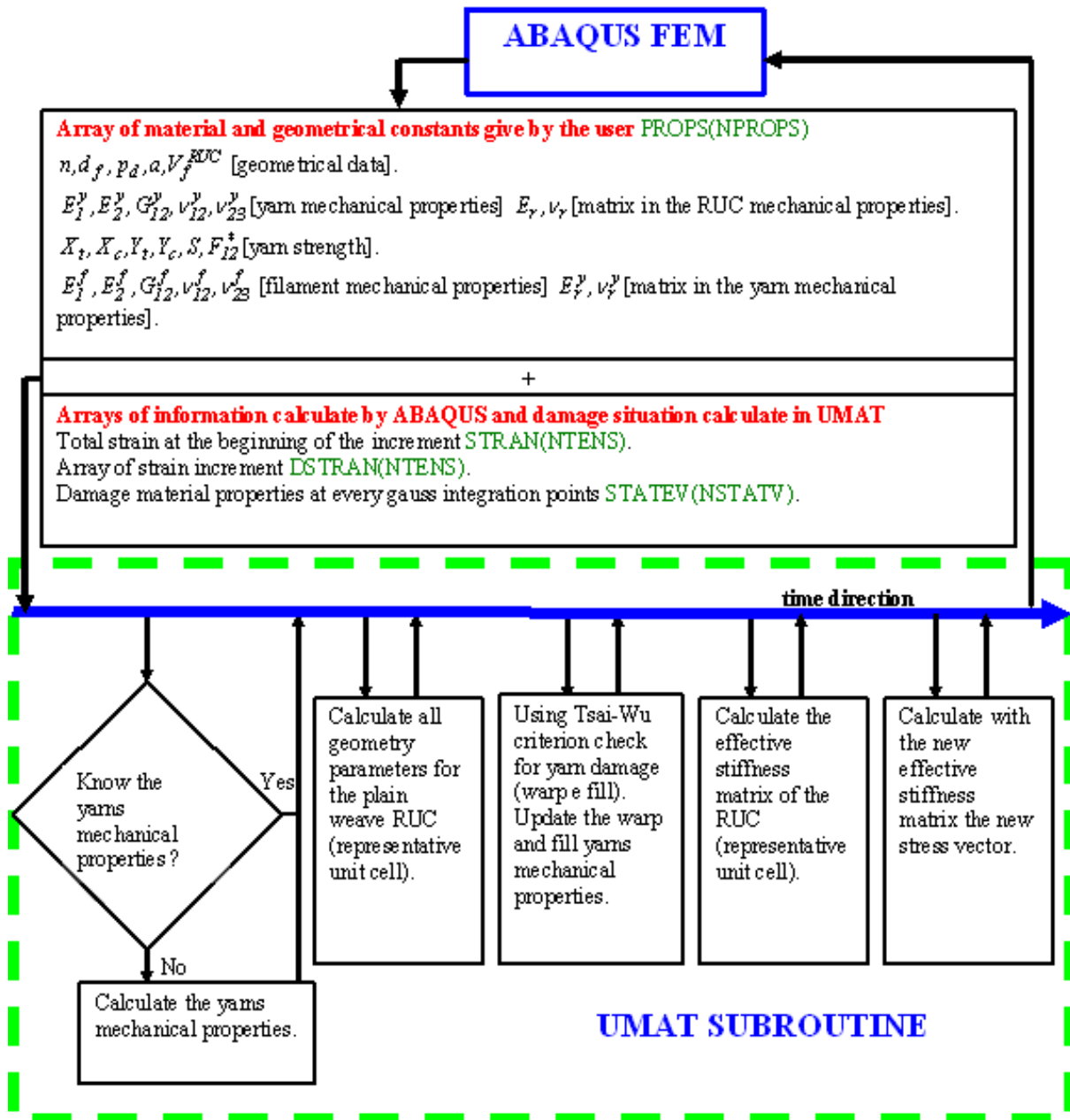


Figure 4.16: Flow chart of the implementation of the code in ABAQUS.

For the $k + 1^{th}$ solution increment, the strains may be written:

$$\varepsilon_{k+1}^i = \varepsilon_k^\infty + \Delta\varepsilon_{k+1}^i \tag{4.19}$$

Where ε_k^∞ represents the strains from the previous k^{th} converged solution increment (denoted by letting the iteration index i go to infinity), $\Delta\varepsilon_{k+1}^i$ represents the increment of strain from the previous k^{th} converged step to the i^{th} iteration of the current $k + 1^{th}$ solution increment, and ε_{k+1}^i represents the estimate of the

strains for the strains for the i^{th} iteration of the current $k + I^{th}$ solution increment. The total strains at the beginning of the increment ε_k^∞ are provided to the subroutine UMAT through the array STRAN(NTENS) while the strain increment $\Delta\varepsilon_{k+1}^i$ are provided through the array DSTRAN(NTENS) where NTEN is the size of the strain component array.

As it is shown in figure 4.16 the current version of the UMAT subroutine requires the user to specify 26 input values that define the geometric and material properties. These values are provided through the array PROPS(NPROPS) in the *USER MATERIAL ABAQUS option.

With these variables passed, the user subroutine UMAT calculated the yarns mechanical properties by taking into consideration the information on the warp and fill yarns failure states that are contained in the array STATEV(NSTATV). Then it is calculated the current total strains for the present iteration by summing the total strains from the previous increment and the corresponding iterative increments of strain.

The yarns in the RUC are discretized into slices and for every slice is calculated the value of the Tsai-Wu quadratic criterion in the strain space (4.9). If a new failure mode is detected the stiffnesses and strengths of the yarns are reduced. With the mechanical properties updated, of the warp and fill yarns, it is calculated the effective stiffness matrix of the RUC. Now it is possible to calculate the stress state, using the reference deformation state defined by the previous converged solution, and the increment of stress computed using the current local stiffness matrix. As result, the stress strain relations are written as:

$$\sigma_{k+1}^i = \sigma_k^\infty + \Delta\sigma_{k+1}^i = \sigma_k^\infty + J_{k+1}^i \cdot \Delta\varepsilon_{k+1}^i \quad (4.20)$$

Where σ_k^∞ represents the stress state at the previous k^{th} converged solution increment, J_{k+1}^i represents the local stiffness matrix for the i^{th} iteration of the current $k + I^{th}$ solution increment.

Example problems have been solved using this user subroutine. We have studied a square panel of side 600 mm and thickness 3.43 mm where all the edges are clamped and the load is a uniform pressure applied to the bottom surface.

The input records for the UMAT subroutine are shown in figure 4.17.

```

** =====
** =====

*DEPVAR
  2,
** UMAT Property Data Definitions
** props(1-8):  $V_f^{RCU}, d_f, a, p_d, n, E_1^y, E_2^y, G_{12}^y$ 
** props(9-16):  $\nu_{12}^y, \nu_{23}^y, E_r, \nu_r, X_t, X_c, Y_t, Y_c$ 
** props(17-24):  $S, F_{12}^*, E_r^y, \nu_r^y, E_1^f, E_2^f, \nu_{12}^f, \nu_{23}^f$ 
** props(25-26):  $G_{12}^f, V_f^y$ 
** =====
*USER MATERIAL, CONSTANTS=26
  0.64, 0.007, 1.411, 0.75, 10000., 0., 11730., 5520.
  0.23, 0.3, 3500., 0.35, 1500., 1500., 40., 246.
  68., -0.5, 3400., 0.35, 258000., 18700., 0.26, 0.35
  19680., 0.7
** =====
** =====

```

Figure 4.17: Input records for the UMAT subroutine.

The full plate was modelled using 10X10 eight node linear brick C3D8I of the ABAQUS element library. The results of the progressive failure method are shown in figure 4.18. For the post processing visualization we used a specific method developed to represent the results of a progressive failure analysis in composite materials [6]. A pressure increase of 0.09 MPa was used for the analyses and the number of load step was 59. In the right top there is the load central deflection graph; on its left it is possible to see the deformation of the plate. In the bottom there are representation of the type and the defect positions. The change in the central deflection respect to the situation without damage around the pressure of 0.63 MPa was due to the start of the filaments breakage failure in the yarns, while the change at 1.48 MPa was imputable to the rapid increase of the filaments failure.

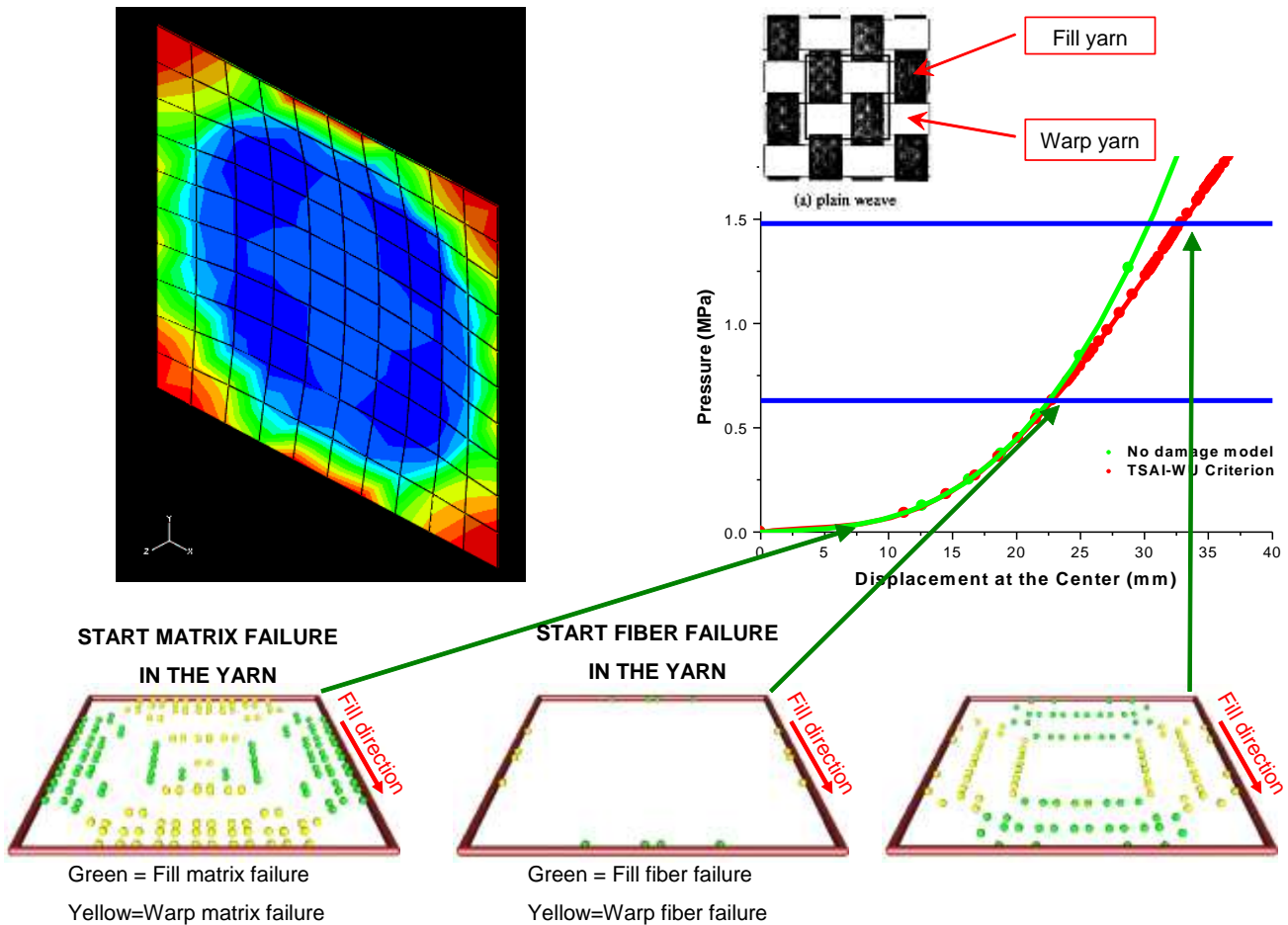


Figure 4.18: Graphical visualization of the results.

5. Validation of the model by testing

The example shown in figure 4.18 was a way to verify the code itself for the presence of macroscopic errors. After this preliminary check was necessary to validate and modify the code using specific experimental results. ENEA in recent years has worked, in collaboration with Italian industry, to create ceramic composite materials.

The aim was to use these materials to validate the code, but preliminary tests have shown insufficient thermal and mechanical characteristics, so we are studying a new strategy of manufacturing to get a better material.

In the meantime, we are studying the results obtained by Japanese colleges for a reference CVI _ SiC/SiC composite shown in part 2 of the final report RP IFERC-R_T1_09-JA-002 [7]. This report refers to a plain weave 2D SiC/SiC composite, fabricated by the CVI method, that we have used as reference material for the verification of the code.

In the report of the Japanese colleagues have been described the guidelines followed for the mechanical characterization of the material with an indication of the geometry used for the specimens.

Figure 5.1 shows typical tensile stress vs. strain relationships for axial tensile loading case (0-degree) and for the off-axial cases (30- and 45-degrees).

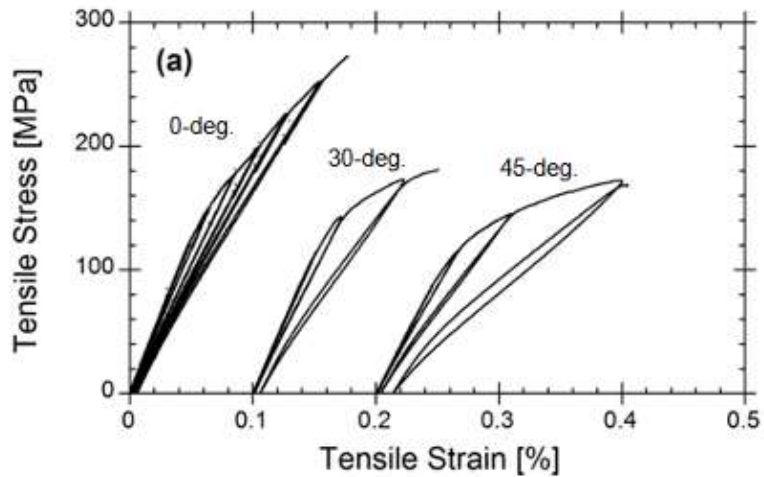


Figure 5.1: Tensile stress vs. tensile curves for reference CVI-SiC/SiC composites.

Figure 5.2 shows a typical stress vs. strain curve of the compression tests.

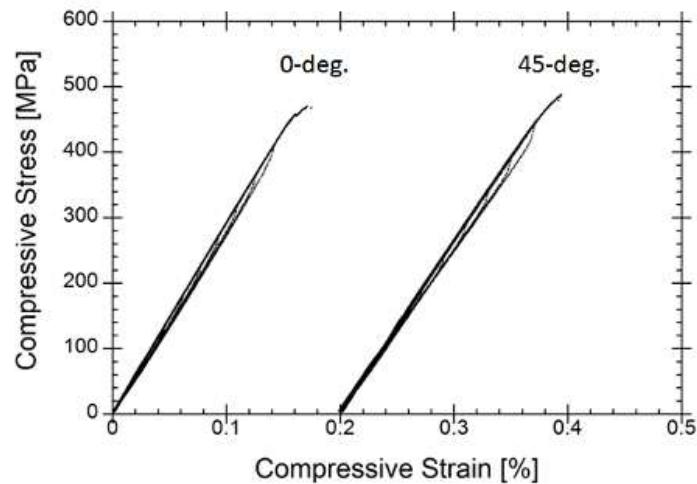


Figure 5.2: Compressive stress vs. compressive strain curves for reference CVI-SiC/SiC composites.

Figure 5.3 shows a typical stress vs. strain curve of the in-plane shear test where the loading angle set apart from the fiber longitudinal direction is 45°.

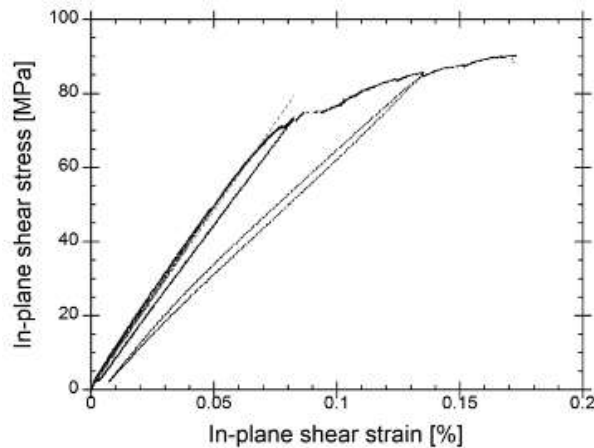


Figure 5.3: In-plane shear stress vs. in-plane shear strain curve for reference CVI-SiC/SiC composites.

Table 5.1 lists the mechanical properties of reference CVI-SiC/SiC composite obtained by the experimental tests.

| Mechanical parameters | Symbol | Value |
|--|------------|---------|
| Axial elastic modulus | E_x | 265 GPa |
| Transverse elastic modulus | E_y | 265 GPa |
| In-plane shear modulus | E_s | 98 GPa |
| Poisson's ratio | ν_{xy} | 0.13 |
| Axial proportional limit tensile stress | X_1 | 117 MPa |
| Transverse proportional limit tensile stress | Y_1 | 117 MPa |
| Axial proportional limit compressive stress | X_1' | 402 MPa |
| Transverse proportional limit compressive stress | Y_1' | 402 MPa |
| Proportional limit in-plane shear stress | S | 67 MPa |
| Axial ultimate tensile stress | X_1 | 272 MPa |
| Transverse ultimate tensile stress | Y_1 | 272 MPa |
| Axial ultimate compressive stress | X_1' | 432 MPa |
| Transverse ultimate compressive stress | Y_1' | 432 MPa |
| Ultimate in-plane shear stress | S | 91 MPa |

Table 5.1: Mechanical parameters of the reference CVI-SiC/SiC composites.

The typical mechanical parameters, used as inputs for the UMAT subroutine, are shown in figure 4.17. Confronting these data with the mechanical data obtained from the experimental tests we can see problems linked to the incomplete knowledge of the input parameters. In fact, the geometrical parameters could be measured, but the filament and matrix mechanical properties are difficult to know. What we have done, to overcome the lack of knowing about the mechanical properties of the single constituents, were to develop a software tool that was able

to assess these mechanical properties taking in consideration the experimental results shown in Table 5.1.

The program was written in Visual Basic and in figure 5.4 is reported the scheme for the insertion of the mechanical properties of the single constituents therefore the filament and matrix in the yarn and the matrix between the yarns that we identify as matrix in the RUC.

The geometrical data are parameters that are know, while a first tentative for the physical data could be obtained from the data sheet of the fibre and using bibliographic result knowing the matrix material.

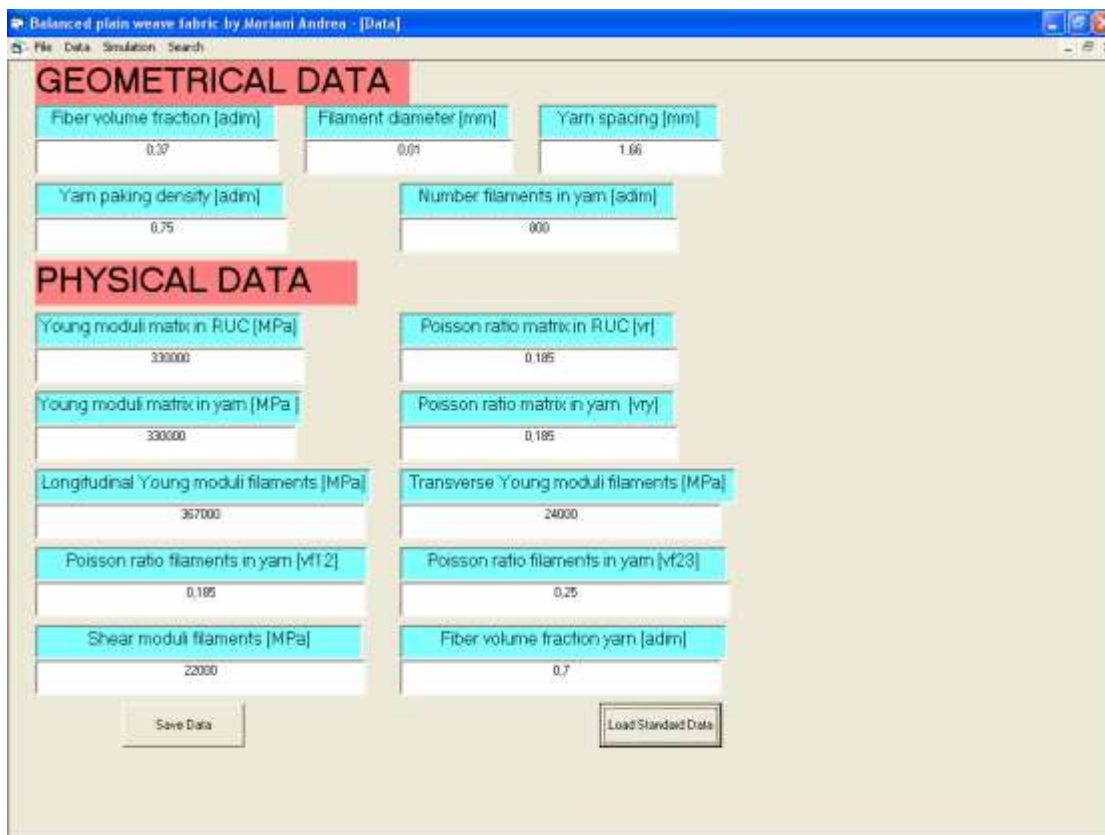


Figure 5.4: Graphical user interface for the data introduction.

After the introduction of the geometry and the physical properties of the single constituents we can open the simulation window (figure 5.5) to calculate the effective moduli of the yarn and the representative unit cell (RUC). In this window it is possible to change every geometrical and mechanical parameters, using specific slide bars and then, pressing the solve button, it is possible calculated the plane weave geometry, the yarn mechanical properties and the plane weave mechanical properties (RUC). The change of the input parameters must be done wisely until it is possible to reproduce the experimental results that for the specific problem are the mechanical properties reported in Table 5.1.

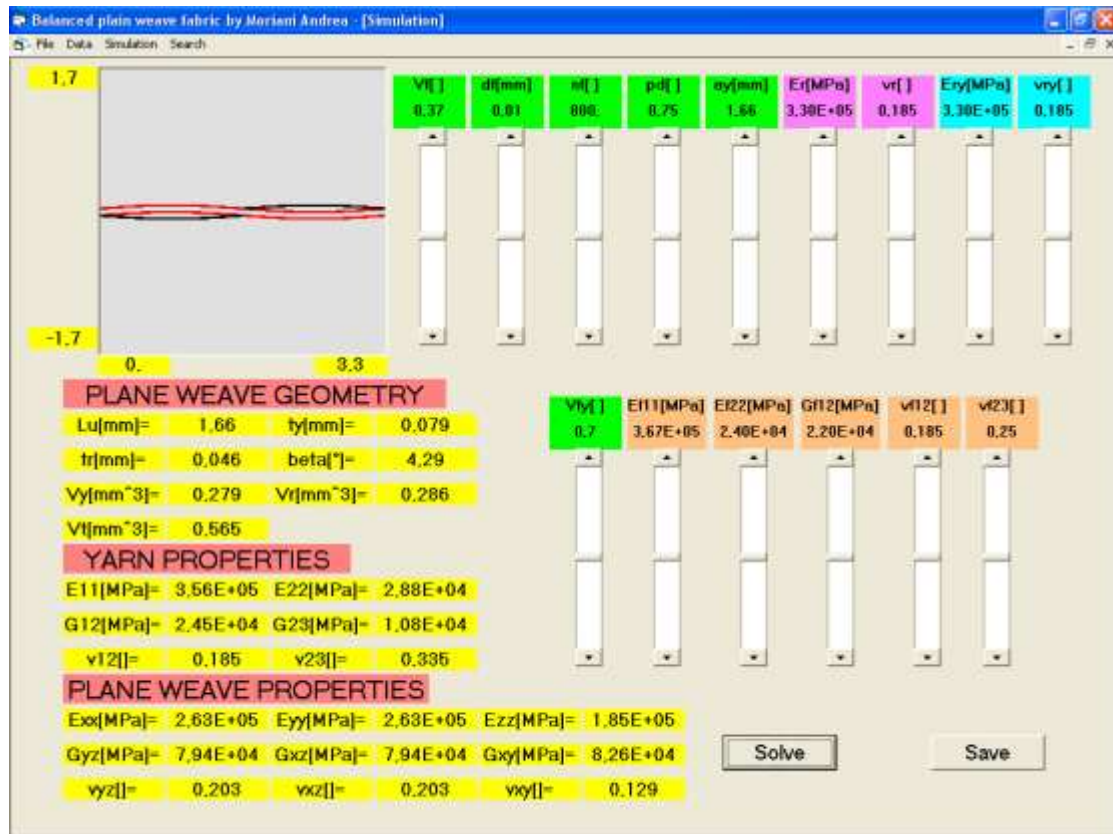


Figure 5.5: Graphical user interface for the moduli calculation.

Using the results of this software tool we have define an input records for the UMAT subroutine that could be taken as representative of the single constituent properties. This new input records for the UMAT subroutine is shown in figure 5.6.

```

** MATERIALS
** =====
** props(1-8): Vf, df, ay, pd, nf, E11, E22, G12,
** props(9-16): v12, v23, Er, vr, XT, XC, YT, YC
** props(17-24): SC, F12STAR, Ery, vry, Efl1, Ef22, vfl2, vfl3
** props(25-26): Gfl2, Vf yarn
** Massimo 8 per fila
** =====
**
**
*Depvar
    2,
*User Material, constants=26
    0.37, 0.010, 1.66, 0.75, 800., 0., 11730., 5520.
    0.23, 0.3, 330000., 0.185, 155., 480., 60., 480.
    25., -0.5, 330000., 0.185, 367000., 24000., 0.185, 0.25
    22000., 0.7
**par_6=0.65

```

Figure 5.6: Input records for the UMAT subroutine.

The use of the UMAT subroutine with the input file shown in figure 5.6, to simulate the experimental tests, has taken to the results shown in figure 5.7.

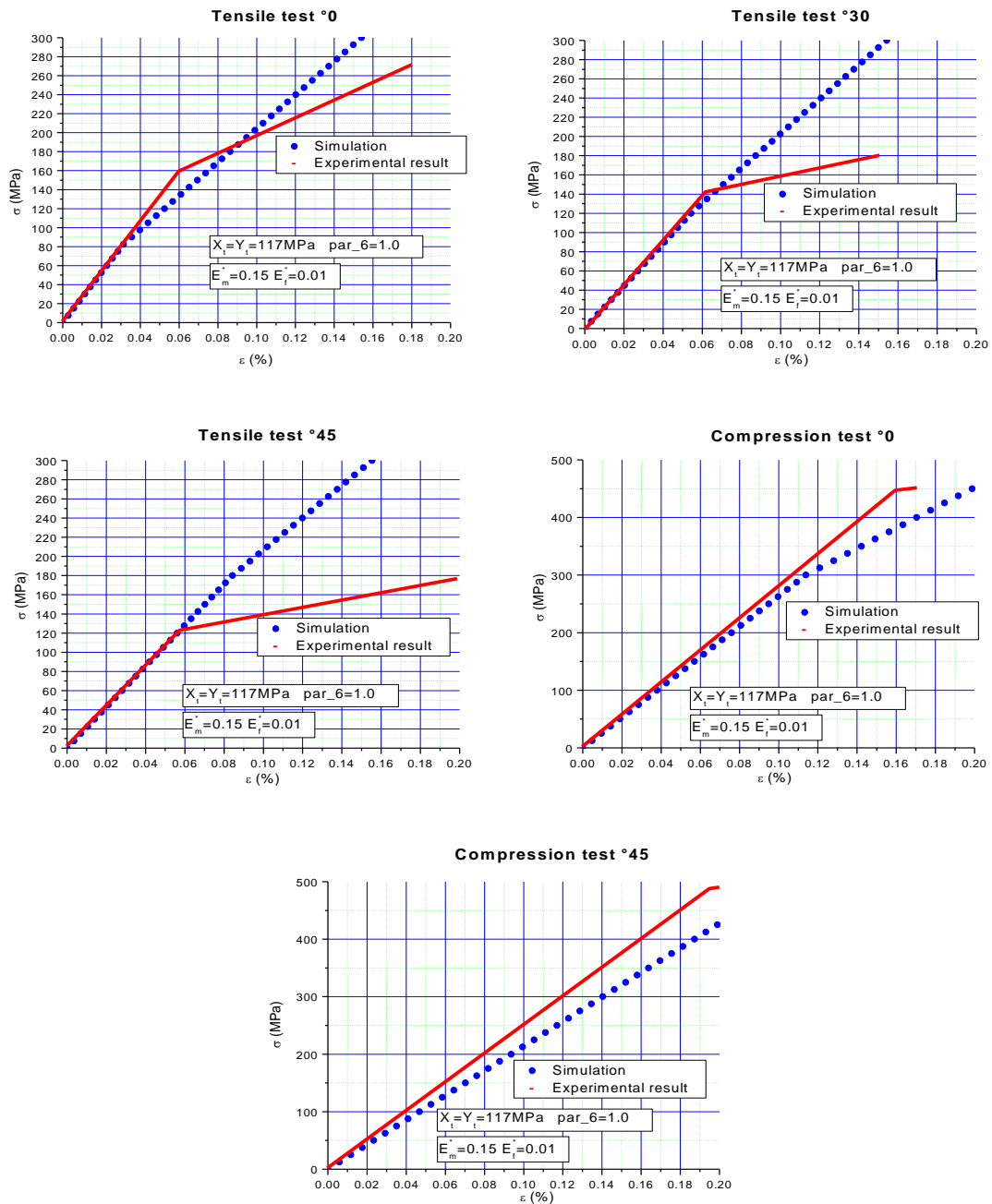


Figure_5.7: Comparison between experimental results and numerical simulation.

In the figure are indicated the values of some parameters used for the numerical simulation, in particular the tensile strength in the yarn direction X_t and in the transverse direction Y_t and the compressive strength in the yarn direction X_c and in the transverse direction Y_c , there are also reported the constants E_m^* and E_f^* , respectively, the matrix and filament degradation factors.

From this comparison was evident that the numerical model needs some consideration:

1. Until now the numerical model takes in consideration damage within the yarns but it doesn't take in consideration for damage in the matrix of the RUC (representative unit cell).
2. The tensile and compression strength until now are referred to the yarns because we are considering damage within the yarns, but the tensile and compression strength gotten from experimental tests and reported in Table 5.1 are referred to the RUC strength.
3. The numerical model used empirical constants, like the partitioning parameters and the degradation factors for the matrix and filament that must be trim on the used materials.

The first consideration bring to introduce in the material failure mechanism also the damage of the matrix in the RUC, while the second consideration shows the necessity to define, inside the material failure model, two different strength parameters, one related to the yarns and the other related to the RUC. Before to update the code we have studied the effect of the values of the strength of the yarn and the effect of the degradation of the RUC matrix stiffness. In figure 5.8 are shown these parameters effect.

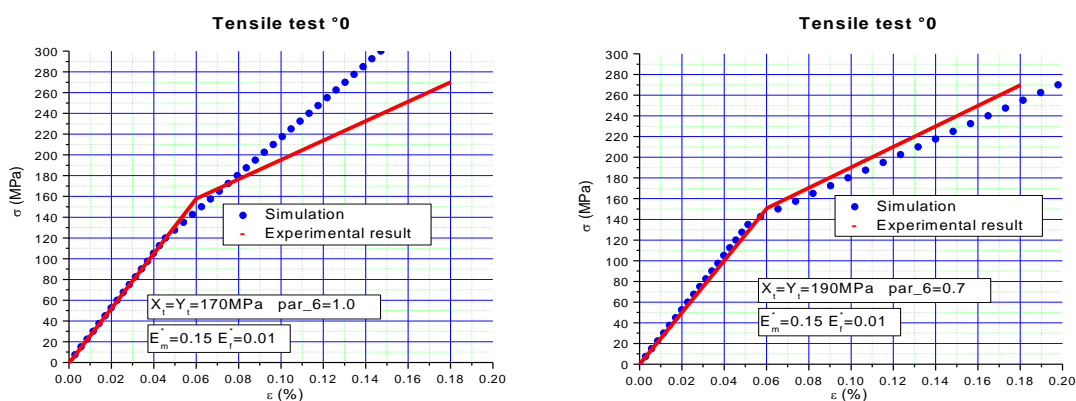


Figure_5.8: Effect of the strength of the yarn and the RUC matrix stiffness.

In the first graph was enhanced the strength of the yarn from 117 MPa (used for the simulation in figure 5.6) to 170 MPa with the effect to increase the change in the slop of the tension curve to high stress. In the second graph was introduced the degradation of the RUC matrix stiffness with the effect of reduce the slope of the tension curve.

In the light of these new findings the model was changed with the following philosophy:

1. The numerical model first checks for damage in the yarns and, if damage is recognized, the model degrades the strengths and stiffness of the yarns.

2. Knowing the actual strength and stiffness of the yarns, the model checks for matrix damage in the RUC. To this purpose we have to introduce in the input records for the UMAT subroutine new strength parameters differentiating between those related to the yarns and those related to the RUC.

The damage assessment in the matrix of the RUC is gotten applying the Tsai-Wu quadratic criterion in the strain space similarly how made for the assessment for the yarns damage. If the Tsai-Wu criterion shows the presence of damage in the RUC the sign of the local normal strain are studied. If the maximum plain strain is positive, and there isn't prior failure, the event is assumed to be a matrix failure inside the RUC. Matrix stiffness, of the RUC, is reduced. The stiffness parameters that are modified in case of damage are: the modulus of elasticity E_r and the Poisson's ratio ν_r of the RUC matrix.

After some test to find the best parameters we have define a new input records for the UMAT subroutine, shown in figure 5.9.

```

** MATERIALS
** =====
** props(1-8): Vf, df, ay, pd, nf, E11, E22, G12,
** props(9-16): v12, v23, Er, vr, XT, XC, YT, YC
** props(17-24): SC, F12STAR, Ery, vry, Ef11, Ef22, vf12, vf23
** props(25-26): Gf12, Vfyarn, XTRUC,XCRUC,YTRUC,TCRUC,SCRUC,F12STARRUC
** Massimo 8 per fila
**=====
*Depvar
  3,
*User Material, constants=32
  0.37, 0.01, 1.66, 0.75, 800., 0., 11730., 5520.
  0.23, 0.3,330000., 0.185, 100., 400., 50., 400.
  25., -0.5,330000., 0.185,367000., 24000., 0.185, 0.25
  22000., 0.7, 200., 400., 200., 400., 67., -0.5
** Param_6=0.3

```

Figure 5.9: Input records for the UMAT subroutine.

How is possible to see comparing the previous input reported in figure 5.6 we have increased the number of the input values that the user have to specify that went from 26 to 32. We have introduced the strengths parameters of the RUC that are: the tensile strength of the RUC $XTRUC$ and $YTRUC$, the compressive strength of the RUC $XCRUC$ and $YCRUC$, the in-plane longitudinal shear strength $SCRUC$ and the coefficient for the interaction term $F12STARRUC$.

We have also increased the number of solution state variables that are associated with this material changing this value from 2 to 3. Therefore the STATEV(NSTATV) that contains the solution-dependent state variables now has three components: the first corresponds to the warp yarn, the second to the fill yarn and the third to

the RUC matrix. We have just described the first two the last could have two values: (1) No failure of the RUC matrix; (2) RCU matrix failure.

The use of the UMAT subroutine with the input file shown in figure 5.9, to simulate the experimental tests, has taken to the results shown in figure 5.10.

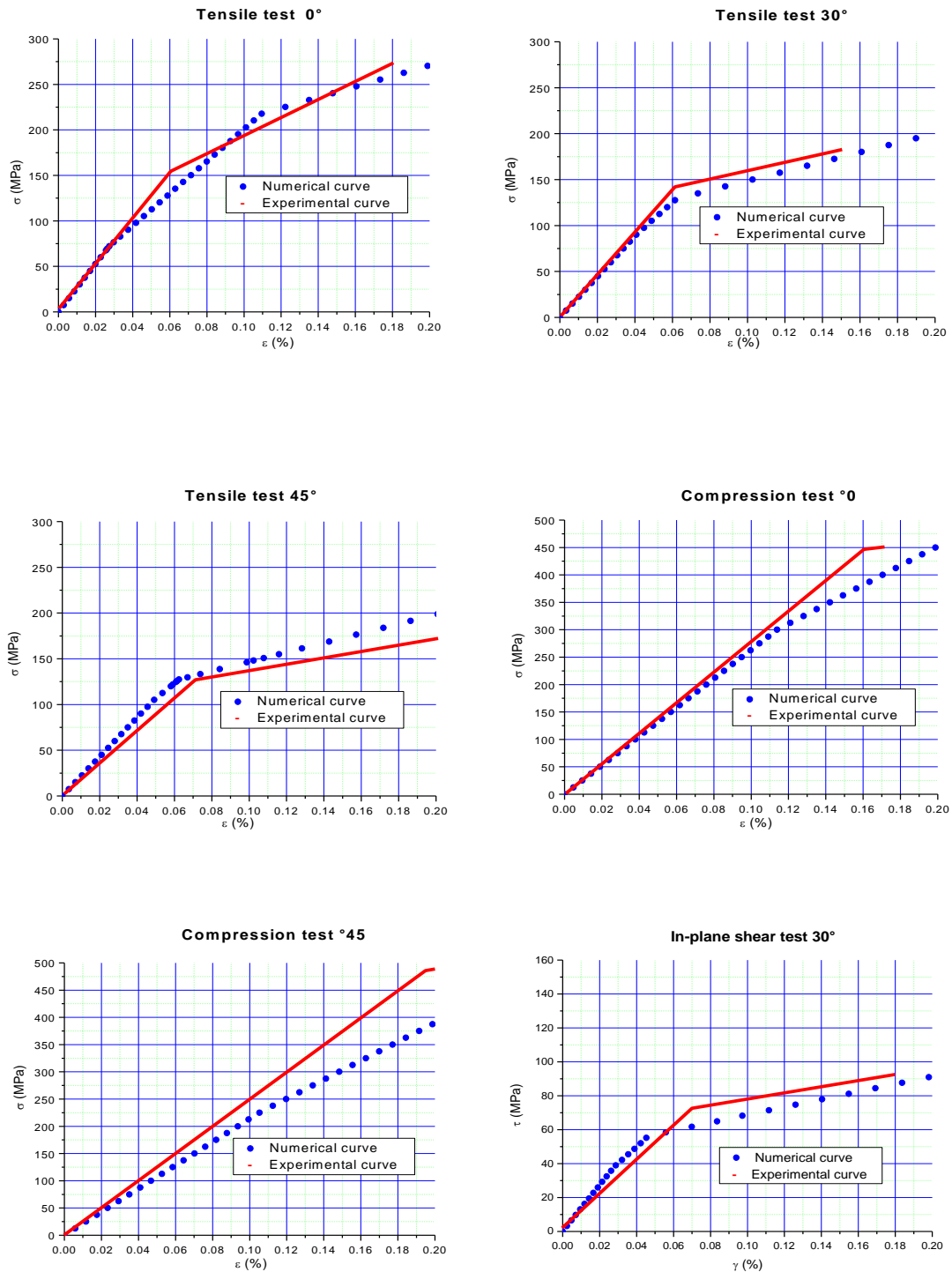


Figure_5.10: Comparison between experimental results and numerical simulation.

The results are in good agreement with the experimental tests. In figure 5.10 is also compared the in-plane shear results gotten with an off-axis specimen test with the numerical results of the tensile off-axis case with 30-degree loading direction. The mechanism of damage was investigated for the tensile test (case 0-degree). In figure 5.11 is shown the numerical results.

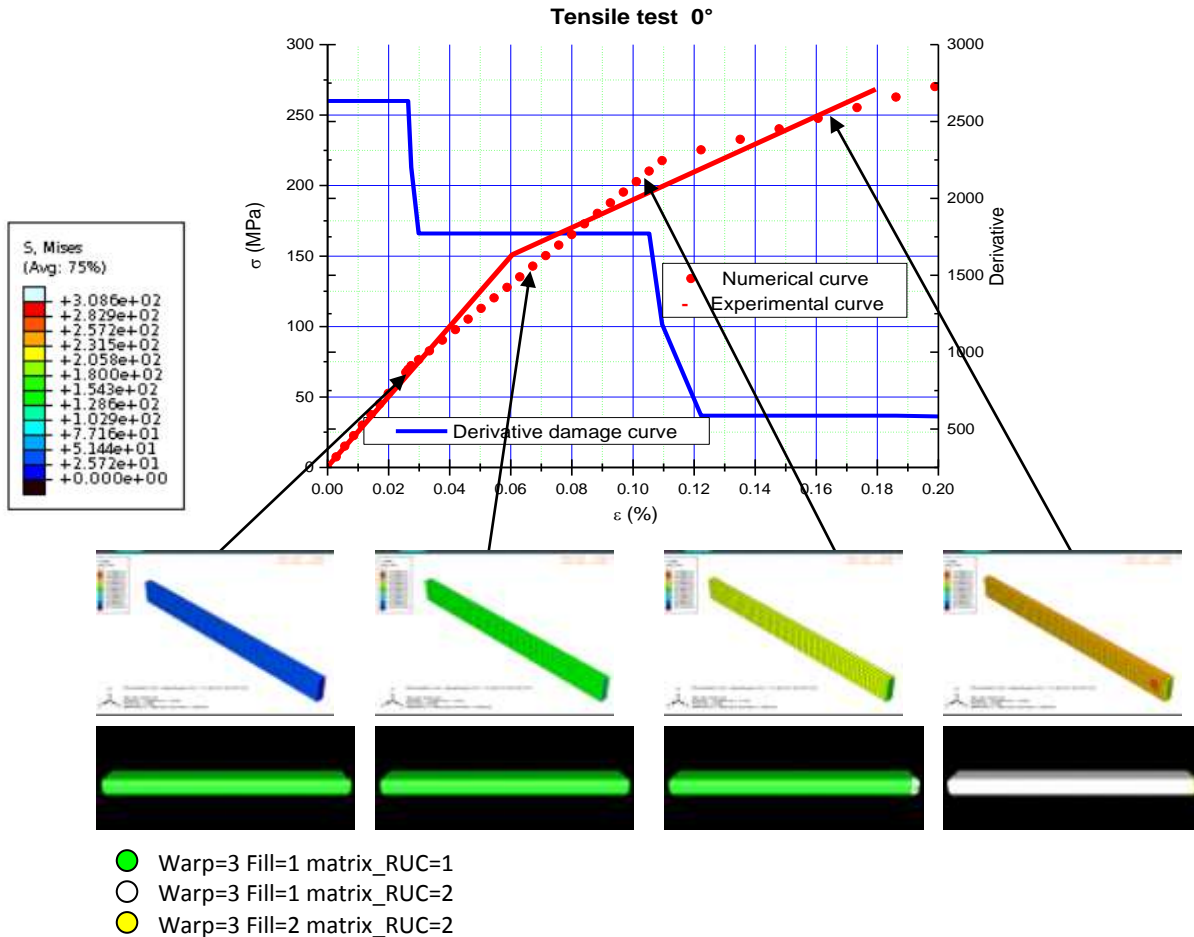


Figure 5.11: Damage mechanism for tension test case 0-degree.

The upper graph shows the tensile stress-strain curve and the derivative of the numerical results. We have studied four specific points where we have visualized the type and position of the damage. The specimen is pull on the left size while it is fix on the right. To the bottom are shown the stress and for more practices the colours legend is enlarged in the middle left of the figure. The figures with black background show the type and position of the damage.

Below there are the colour legend that specify the type of damage. The meaning of the three numbers has been already described, but for convenience will repeat the meaning:

1. The first number is referred to the warp yarn and can have four values:

- (1) No damage.
 - (2) Matrix inside the warp yarn damaged.
 - (3) Filament inside the warp yarn damaged.
 - (4) Matrix damage followed by filament damage in the warp yarn.
2. The second number is referred to the fill yarn and can have four values:
- (1) No damage.
 - (2) Matrix inside the fill yarn damaged.
 - (3) Filament inside the fill yarn damaged.
 - (4) Matrix damage followed by filament damage in the fill yarn.
3. The third number is referred to the matrix of the RUC and it can have two values:
- (1) No damage.
 - (2) Matrix of the RUC damaged.

The first damage arises in the filaments of the warp yarns and it is uniformly distributed. Then at the fix, the damage in the matrix of the RUC, starts and grows with the increase of the load, interesting the all materials. At the end the matrix damage in the fill yarns starts too, always in the fixed position.

A similar study was done also for the tensile test (case 30-degree) and the compression test (case 0-degree). In figures 5.12 and 5.13 are shown, respectively, the results.

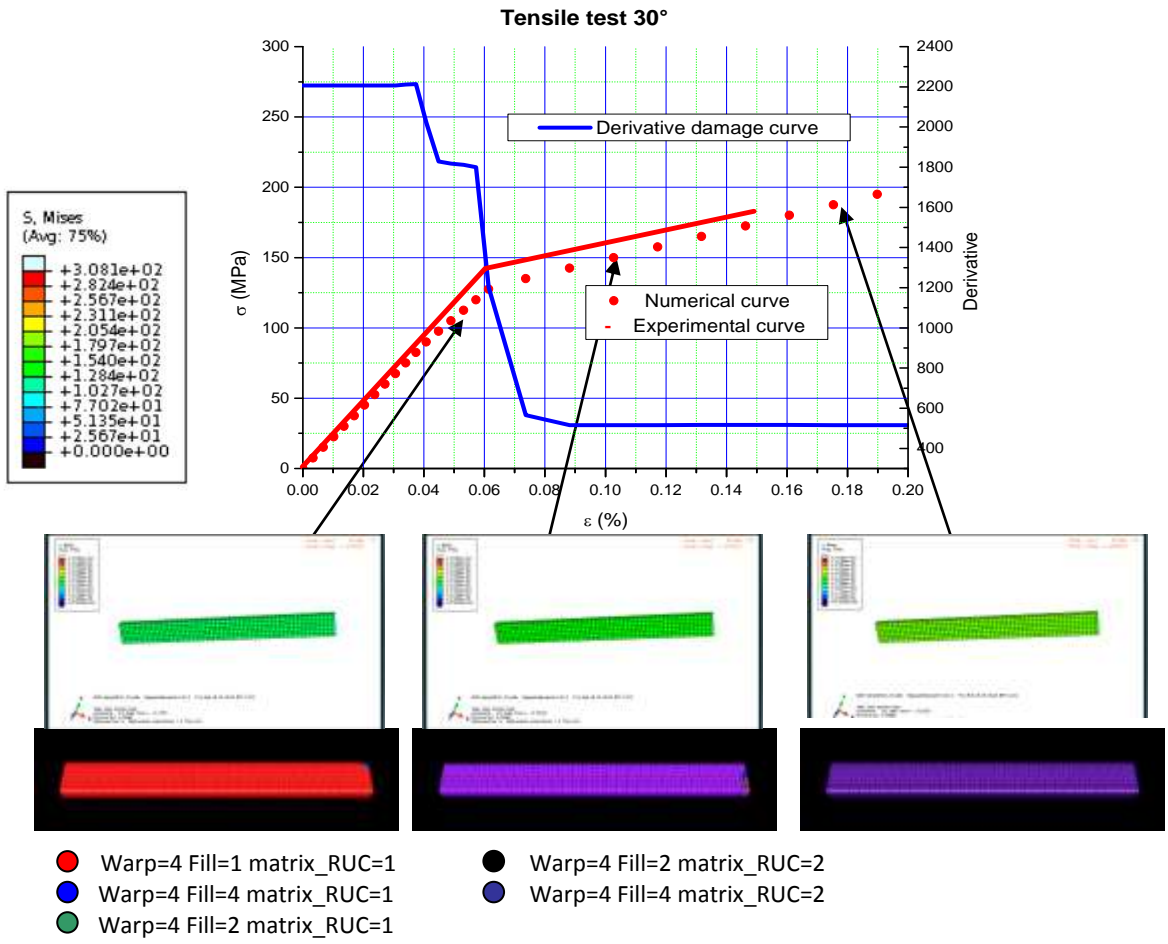


Figure 5.12: Damage mechanism for tension test case 30-degree.

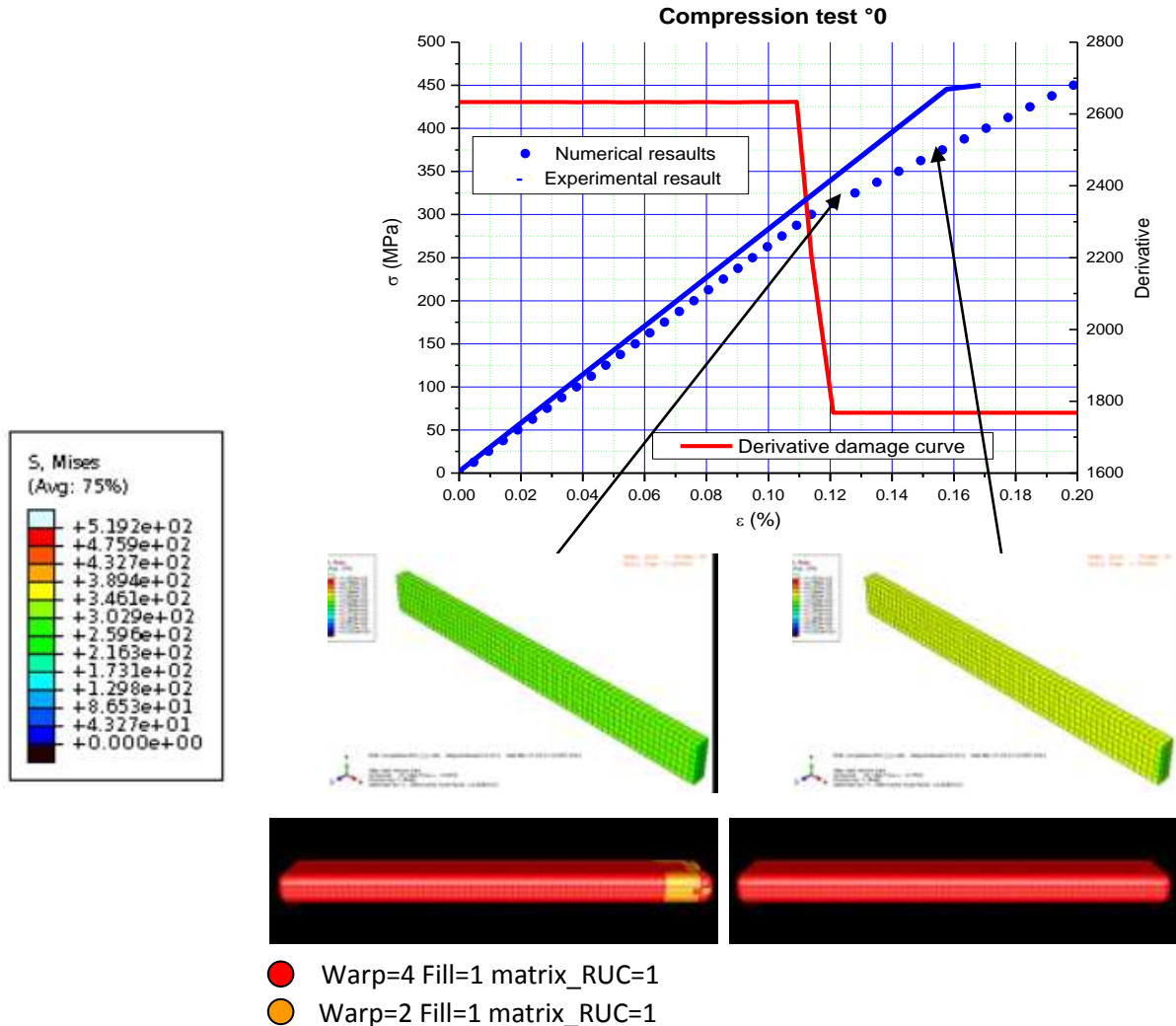


Figure 5.13: Damage mechanism for compression test case 0-degree.

In both the cases the damage is uniformly distributed and specific behaviours could be localized in the fixed position.

The numerical study of the tension tests has shown other interesting considerations that are in agreement with the behaviours of the anisotropic materials. For the cases of tensile load 0 degrees and 45 degrees the symmetric behaviour with respect to the direction of load shows no bending of the specimens and the displacements are along the loading direction, as shown in figure 5.14.

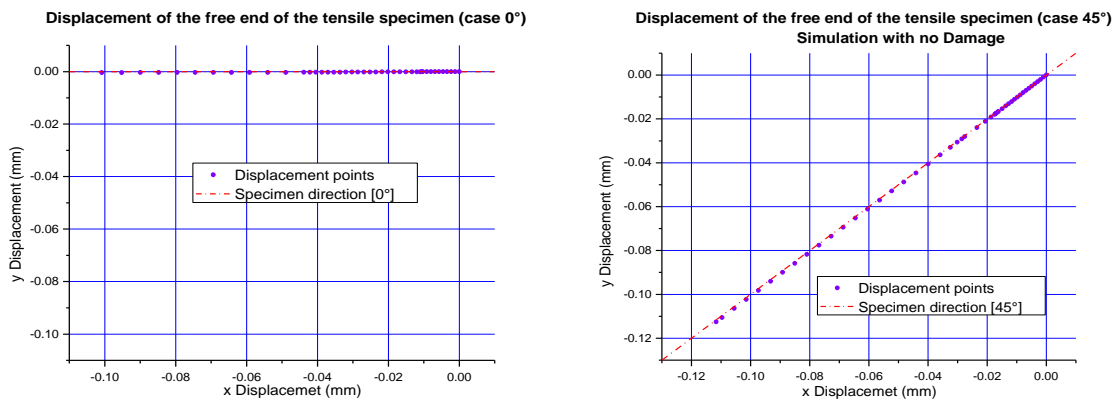


Figure 5.14: Displacement of the free end of the tensile specimens 0-degree and 45-degree.

For the case of tensile load 30 degrees the non symmetric behaviour with respect to the direction of load determines a situation where the displacement of the free end of the specimen doesn't follow the direction of load so the specimen bent. This behaviours are shown in figure 5.15 where are reported the cases with no damage and with damage. The ends free of the specimen follow a direction which is 10° shifted relative to the direction of loading. For the case in which is not taken into account damage the displacement direction does not change during the increase of the load (10° shifted relative to the direction of loading), while in the case in which it is taken into account damage the displacement direction first tends to follow the direction which is 10° shifted relative to the direction of loading, but then with the beginning of damage the displacement direction tends to follow the direction of the load.

In the figures 5.14 and 5.15 the warp yarns are in the x direction and the fill yarns are in the y direction.

This behaviours could be confirm applying the classical laminate theory to a specific composite, made by stacking together unidirectional plies oriented in specific directions, to reproduce the specimens that were used for the axial tensile loading case and the off-axial tensile load cases.

These studies are made in Appendix 1 where we have study tree specimens with the follow staking sequences:

1. $(0^\circ/90^\circ)_s$ to study the tensile case 0-degree.
2. $(45^\circ/-45^\circ)_s$ to study the tensile case 45-degree.
3. $(30^\circ/-60^\circ)_s$ to study the tensile case 30-degree.

The results of these study show that for the first two cases we have only strains in the x and y direction, while in the third case we have also shear strain that determines a bent of the specimen in the x y plane confirming what we have found in our study.

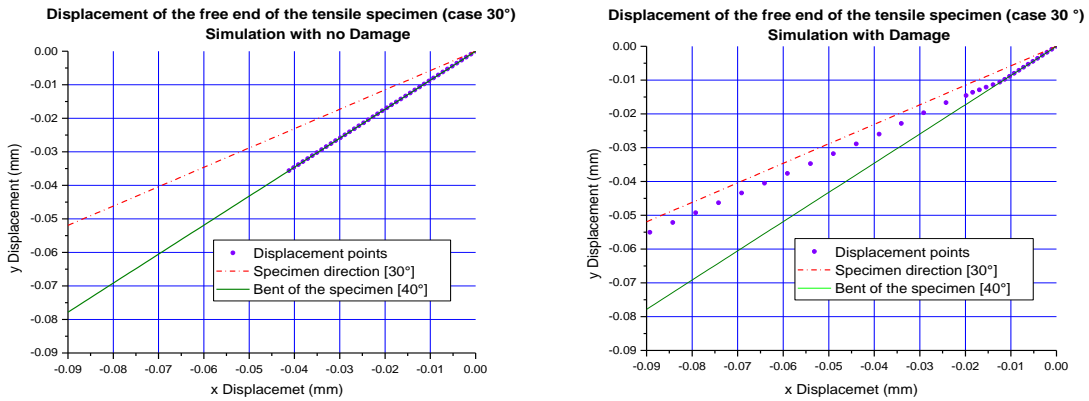
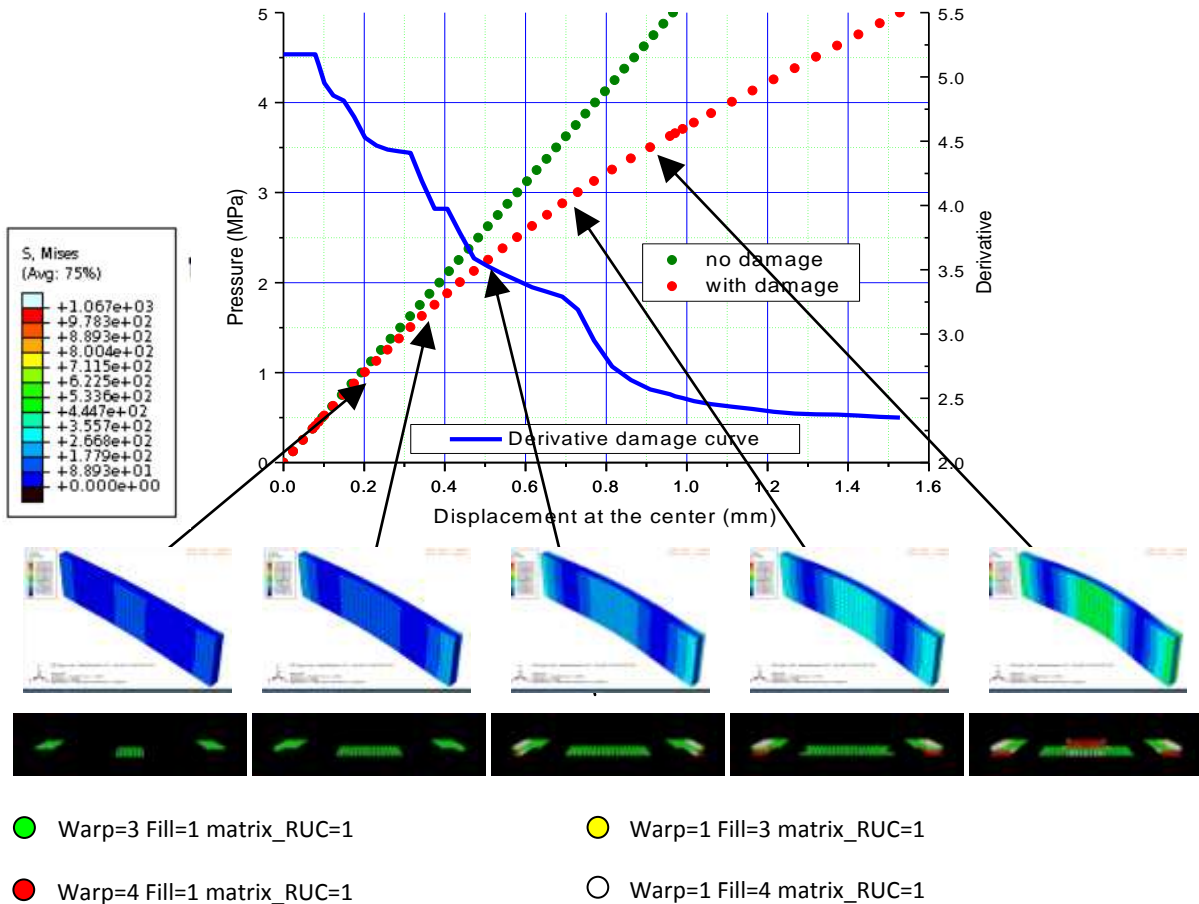


Figure 5.15: Displacement of the free end of the tensile specimen 30-degree.

Using the same input record for the UMAT subroutine we have studied other two example problems that could be used for further validation of the code. The first was a beam with length 200 mm, wide 50 mm and thickness 10 mm where both the edges along the wide are clamped and the load is a uniform pressure applied to the upper surface. The results of the progressive failure method are shown in figure 5.16.



- Warp=3 Fill=1 matrix_RUC=1
- Warp=1 Fill=3 matrix_RUC=1
- Warp=4 Fill=1 matrix_RUC=1
- Warp=1 Fill=4 matrix_RUC=1

Figure 5.16: Damage mechanism for the beam example.

In the upper part, of the figure 5.16, there is the load central deflection graph; below there are the stresses distribution associated with the representation of the type and the defect positions.

In this example is possible to see that the damage started where the materials are in a tension stresses. The damage then grows, with the increase of the pressure, in the clamped and central part of the beam where the stresses are higher.

The second example was a plate with the same geometry used in figure 2.1, i.e. a square panel of side 600 mm and thickness 3.43 mm where all the edges are clamped and the load is a uniform pressure applied to the upper surface. The results of the progressive failure method are shown in figure 5.17.

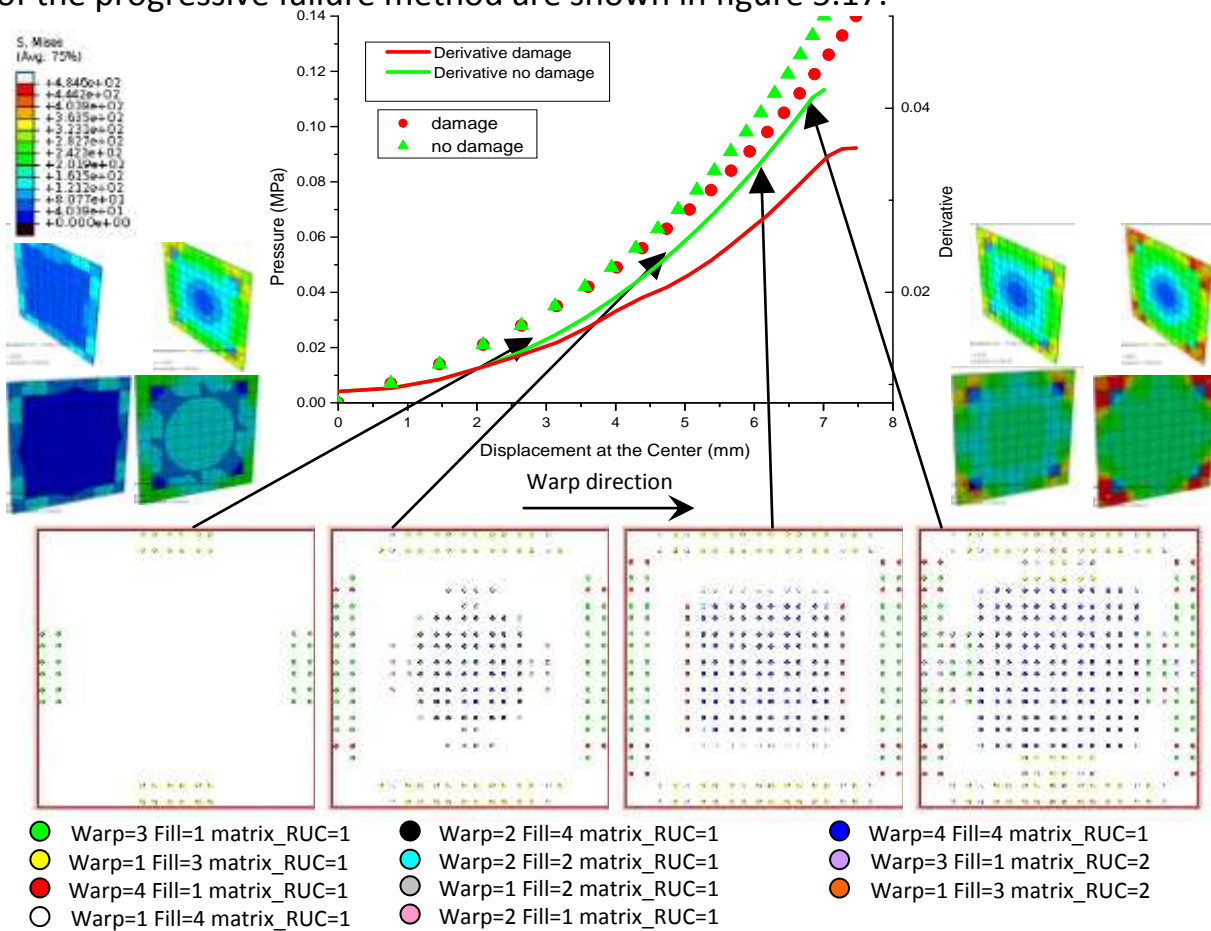


Figure 5.17: Damage mechanism for the square panel example.

In the upper part, of the figure 5.17, there is the load central deflection graph; below there are the stresses distribution in both side of the plate associated with the representation of the type and the defect positions. The change in the central deflection respect to the situation without damage around the pressure of 0.03 MPa

was due to the start of the filaments breakage failure in the fill and warp yarns. The position was near the edge of the plate.

A rapid change in the central deflection around the pressure of 0.06 MPa was due to the start and a rapid increase of the matrix and filament failure of the fill and warp yarns in the centre of the plate. Then, with the increase of the pressure, even in the region between the centre and the edges of the plate are beginning to occur damage of the filament of the fill and warp yarns.

6. Conclusions

In this paper, was studied a multiscale methodology for composite structural modelling. The first part was used to implement a progressive failure method into the general purpose finite element program, ABAQUS and to develop a specific application for a post processing visualization of the results. This introductory work was a way to understand the capability given from the commercial code and it allows also to integrate this code with a specific tool, to represent the results of the analysis answering to questions, like where is the first ply failure and how the progression of the damage develops. The strong limitations in the standard finite element codes, studying composite materials using multiscale methodology, have led us to seek commercial codes that were able to add the necessary micro-scale analysis in a standard finite element software.

There aren't many codes based on computational composite engineering micromechanics. They are almost totally developed from the NASA (National Aeronautics and Space Administration) and when commercialized they are characterized by exorbitant costs. One of these codes is GENOA-PFDA (Progressive Failure Dynamic Analysis) that, applying the hierarchical modelling, calculates the stress-strain field at micro-scale level using micromechanics and calculating for possible damage in the volume elements of the unit cell. Once damage, at the unit cell level, has been detected the code degrades the relevant fiber/matrix mechanical properties.

The high cost of the commercial code has brought us to the decision to internally develop a multiscale code based on the commercial software ABAQUS. We have developed a constitutive model for balanced plain weave fabric and we have also implemented the micromechanical model, writing a specific user material subroutine for ABAQUS, called UMAT.

This code resolves the geometry and it can calculate the equivalent elasticity matrix to a balanced plain weave fabric. We have also determined a material failure mechanism theory for the balanced plain weave architecture, which takes in consideration damage within the yarns and also in the matrix of the RUC (representative unit cell).

For validate the code we have used results obtained by the Japanese colleagues for a reference CVI- SiC/SiC composites shown in part 2 of the final report RP IFERC-R-T1-09-JA-002. This report refers to a plain-weave 2D SiC/SiC composite, fabricated by the CVI method which was suitable for the code validation. During this phase the code was updated and it was also developed specific software tool, which asses the mechanical properties of single constituents that reproduce the experimental results related to the RUC.

After this phase of update we have reproduced, with the code, the experimental tests as axial and off-axial tensile test, compressive and in-plane shear tests. The numerical results are in good agreement with the experimental tests and also the considerations on the type and progression of the damage seem to be in good agreement with the real behaviour. Also the study of the displacement of the free end of the specimens in the tensile tests is in agreement with what one would expect to be.

Finally we have simulated two cases that could be used to make a further validation of the code. In these tests we have multi-axial stresses so they could represent an interesting test case for the code.

Appendix 1

Classical laminate theory applied to tensile load tests

We take unidirectional laminae with the following mechanical properties derived by applying the rule of mixtures to the matrix in the RUC and the yarns mechanical properties, gotten using the software tools described in figure 5.4 and 5.5:

$$E_{11} = 340.0GPa, E_{22} = 67.8GPa, G_{12} = 51.0GPa, \nu_{12} = 0.185$$

Where:

E_{11} is the elastic modulus in the fiber direction or longitudinal direction,

E_{22} is the elastic modulus in the transverse fiber direction,

G_{12} is the shear modulus in the 1-2 axes,

ν_{12} is the Poisson's ratio,

The compliance matrix is:

$$S = \begin{bmatrix} \frac{1}{E_{11}} & -\frac{\nu_{21}}{E_{22}} & 0 \\ -\frac{\nu_{12}}{E_{11}} & \frac{1}{E_{22}} & 0 \\ 0 & 0 & \frac{1}{G_{12}} \end{bmatrix} \quad (A1.1)$$

The stiffness matrix is:

$$C = S^{-1} \quad (A1.2)$$

The ply can be rotated in the stacking sequence of an angle θ so the transformed stiffness matrix is:

$$\bar{C} = T^{-1} * C * R * T * R^{-1} \quad (A1.3)$$

Where:

$$T = \begin{bmatrix} \cos^2 \theta & \sin^2 \theta & 2 * \cos \theta * \sin \theta \\ \sin^2 \theta & \cos^2 \theta & -2 * \cos \theta * \sin \theta \\ -\cos \theta * \sin \theta & \cos \theta * \sin \theta & \cos^2 \theta - \sin^2 \theta \end{bmatrix} \quad (A1.4)$$

It is the transformation matrix.

$$R = \begin{bmatrix} 1 & 0 & 0 \\ 0 & 1 & 0 \\ 0 & 0 & 2 \end{bmatrix} \quad (\text{A1.5})$$

It is the Reuter's matrix that takes in consideration that the classical definition of the shear strain is twice the tensorial shear strain.

At this point we are able to study situations when the stresses and material principal directions are aligned and also when these two set of axes are not aligned.

Now we can use those results to formulate the behaviour of a laminate through the plate constitutive equations:

$$\begin{bmatrix} N \\ M \end{bmatrix} = \begin{bmatrix} A & B \\ A & D \end{bmatrix} * \begin{bmatrix} \varepsilon^0 \\ k \end{bmatrix} \quad (\text{A1.6})$$

Where:

N are the external forces per unit width,
 M are the external moments per unit width,
 ε^0 is the in plane strains,
 k is the plate curvatures,

The element of the laminate stiffness matrix is:

$$\begin{aligned} A_{rs} &= \sum_{j=1}^p \overline{C_{rsj}} * (h_j - h_{j-1}) \\ B_{rs} &= \frac{1}{2} * \sum_{j=1}^p \overline{C_{rsj}} * (h_j^2 - h_{j-1}^2) \\ D_{rs} &= \frac{1}{3} * \sum_{j=1}^p \overline{C_{rsj}} * (h_j^3 - h_{j-1}^3) \end{aligned} \quad (\text{A1.7})$$

Where p is the number of plies and $h_j - h_{j-1} = t_j$ is the thickness of the layer j .

Using the equation (A1.6) we can impose to the specimen a force of traction and, knowing the stacking sequence, we can build the stiffness matrix, so we are able to determine the strains vector and therefore understand the type of displacement of the specimen.

1. Case (0°/90°)_s:

The stiffness matrix for $\theta = 0^\circ$ and $\theta = 90^\circ$ are:

$$C_{0^\circ} = \begin{bmatrix} 3.423 \cdot 10^5 & 1.263 \cdot 10^4 & 0 \\ 1.263 \cdot 10^4 & 6.827 \cdot 10^4 & 0 \\ 0 & 0 & 5.1 \cdot 10^4 \end{bmatrix} \quad [MPa] \quad (A1.8)$$

$$C_{90^\circ} = \begin{bmatrix} 6.827 \cdot 10^4 & 1.263 \cdot 10^4 & 0 \\ 1.263 \cdot 10^4 & 3.423 \cdot 10^5 & 0 \\ 0 & 0 & 5.1 \cdot 10^4 \end{bmatrix}$$

The elements of the laminate stiffness matrix are:

$$A = \begin{bmatrix} 1.027 \cdot 10^5 & 6.315 \cdot 10^3 & 0 \\ 6.315 \cdot 10^3 & 1.027 \cdot 10^5 & 0 \\ 0 & 0 & 2.55 \cdot 10^4 \end{bmatrix} \quad \left[\frac{N}{mm} \right]$$

$$B = \begin{pmatrix} 0 & 0 & 0 \\ 0 & 0 & 0 \\ 0 & 0 & 0 \end{pmatrix} \quad [N] \quad (A1.9)$$

$$D = \begin{bmatrix} 3.209 \cdot 10^3 & 131.554 & 0 \\ 131.554 & 1.068 \cdot 10^3 & 0 \\ 0 & 0 & 531.25 \end{bmatrix} \quad [N * mm]$$

Therefore:

$$\begin{pmatrix} A & B \\ B & D \end{pmatrix} = \begin{bmatrix} 1.027 \cdot 10^5 & 6.315 \cdot 10^3 & 0 & 0 & 0 & 0 \\ 6.315 \cdot 10^3 & 1.027 \cdot 10^5 & 0 & 0 & 0 & 0 \\ 0 & 0 & 2.55 \cdot 10^4 & 0 & 0 & 0 \\ 0 & 0 & 0 & 3.209 \cdot 10^3 & 131.554 & 0 \\ 0 & 0 & 0 & 131.554 & 1.068 \cdot 10^3 & 0 \\ 0 & 0 & 0 & 0 & 0 & 531.25 \end{bmatrix} \quad (A1.10)$$

Using the (A1.6) equation is possible to determine the strain vector imposing a traction force therefore:

$$\begin{pmatrix} N \\ M \end{pmatrix} = \begin{bmatrix} N_x \\ N_y \\ N_{xy} \\ M_x \\ M_y \\ M_{xy} \end{bmatrix} = \begin{bmatrix} 100 \\ 0 \\ 0 \\ 0 \\ 0 \\ 0 \end{bmatrix} \quad (A1.11)$$

$$\begin{pmatrix} \varepsilon^0 \\ \kappa \end{pmatrix} = \begin{bmatrix} \varepsilon_x^0 \\ \varepsilon_y^0 \\ \gamma_{xy}^0 \\ \kappa_x \\ \kappa_y \\ \kappa_{xy} \end{bmatrix} = \begin{pmatrix} A & B \\ B & D \end{pmatrix}^{-1} \cdot \begin{pmatrix} N \\ M \end{pmatrix} = \begin{bmatrix} 9.778791 \cdot 10^{-4} \\ -6.015467 \cdot 10^{-5} \\ 0 \\ 0 \\ 0 \\ 0 \end{bmatrix}$$

We have longitudinal deformation (in the direction of the force) accompanied by a lateral deformation in the opposite sense. The deformed specimen is shown in figure A.1.

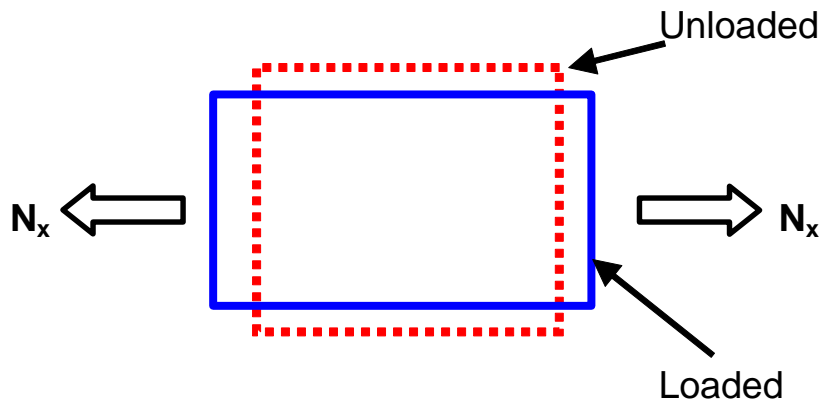


Figure A.1: Deformation of specimen discussed in cases $(0^\circ/90^\circ)_s$ and $(45^\circ/-45^\circ)_s$.

2. Case $(45^\circ/-45^\circ)_s$:

The stiffness matrix for $\theta = 45^\circ$ and $\theta = -45^\circ$ are:

$$C_{-45^\circ} = \begin{bmatrix} 1.6 \cdot 10^5 & 5.797 \cdot 10^4 & 6.852 \cdot 10^4 \\ 5.797 \cdot 10^4 & 1.6 \cdot 10^5 & 6.852 \cdot 10^4 \\ 6.852 \cdot 10^4 & 6.852 \cdot 10^4 & 9.634 \cdot 10^4 \end{bmatrix} \quad [MPa] \quad (A1.12)$$

$$C_{45^\circ m} = \begin{bmatrix} 1.6 \cdot 10^5 & 5.797 \cdot 10^4 & -6.852 \cdot 10^4 \\ 5.797 \cdot 10^4 & 1.6 \cdot 10^5 & -6.852 \cdot 10^4 \\ -6.852 \cdot 10^4 & -6.852 \cdot 10^4 & 9.634 \cdot 10^4 \end{bmatrix}$$

The elements of the laminate stiffness matrix are:

$$A = \begin{bmatrix} 7.998 \cdot 10^4 & 2.898 \cdot 10^4 & 0 \\ 2.898 \cdot 10^4 & 7.998 \cdot 10^4 & 0 \\ 0 & 0 & 4.817 \cdot 10^4 \end{bmatrix} \quad \left[\frac{N}{mm} \right]$$

$$B = \begin{bmatrix} 0 & 0 & 0 \\ 0 & 0 & 0 \\ 0 & 0 & 0 \end{bmatrix} \quad [N] \quad (A1.13)$$

$$D = \begin{bmatrix} 1.666 \cdot 10^3 & 603.804 & 535.294 \\ 603.804 & 1.666 \cdot 10^3 & 535.294 \\ 535.294 & 535.294 & 1.003 \cdot 10^3 \end{bmatrix} \quad [N * mm]$$

Therefore:

$$\begin{pmatrix} A & B \\ B & D \end{pmatrix} = \begin{bmatrix} 7.998 \cdot 10^4 & 2.898 \cdot 10^4 & 0 & 0 & 0 & 0 \\ 2.898 \cdot 10^4 & 7.998 \cdot 10^4 & 0 & 0 & 0 & 0 \\ 0 & 0 & 4.817 \cdot 10^4 & 0 & 0 & 0 \\ 0 & 0 & 0 & 1.666 \cdot 10^3 & 603.804 & 535.294 \\ 0 & 0 & 0 & 603.804 & 1.666 \cdot 10^3 & 535.294 \\ 0 & 0 & 0 & 535.294 & 535.294 & 1.003 \cdot 10^3 \end{bmatrix} \quad (A1.14)$$

Using the (A1.6) equation is possible to determine the strain vector imposing a traction force therefore:

$$\begin{pmatrix} N \\ M \end{pmatrix} = \begin{bmatrix} N_x \\ N_y \\ N_{xy} \\ M_x \\ M_y \\ M_{xy} \end{bmatrix} = \begin{bmatrix} 100 \\ 0 \\ 0 \\ 0 \\ 0 \\ 0 \end{bmatrix} \quad (A1.15)$$

$$\begin{pmatrix} \varepsilon^0 \\ \gamma_{xy}^0 \\ k_x \\ k_y \\ k_{xy} \end{pmatrix} = \begin{pmatrix} A & B \\ B & D \end{pmatrix}^{-1} \cdot \begin{pmatrix} N \\ M \end{pmatrix} = \begin{pmatrix} 0.001 \\ -5.215 \cdot 10^{-4} \\ 0 \\ 0 \\ 0 \end{pmatrix}$$

We have longitudinal deformation (in the direction of the force) accompanied by a lateral deformation in the opposite sense. The deformed specimen is shown in figure A.1.

3. Case (30°/-60°):

The stiffness matrix for $\theta = 30^\circ$ and $\theta = -60^\circ$ are:

$$C_{30^\circ} = \begin{bmatrix} 2.398 \cdot 10^5 & 4.663 \cdot 10^4 & 7.897 \cdot 10^4 \\ 4.663 \cdot 10^4 & 1.028 \cdot 10^5 & 3.971 \cdot 10^4 \\ 7.897 \cdot 10^4 & 3.971 \cdot 10^4 & 8.5 \cdot 10^4 \end{bmatrix} \quad [MPa] \quad (A1.16)$$

$$C_{-60^\circ m} = \begin{bmatrix} 1.028 \cdot 10^5 & 4.663 \cdot 10^4 & -3.971 \cdot 10^4 \\ 4.663 \cdot 10^4 & 2.398 \cdot 10^5 & -7.897 \cdot 10^4 \\ -3.971 \cdot 10^4 & -7.897 \cdot 10^4 & 8.5 \cdot 10^4 \end{bmatrix}$$

The elements of the laminate stiffness matrix are:

$$A = \begin{bmatrix} 8.565 \cdot 10^4 & 2.332 \cdot 10^4 & 9.816 \cdot 10^3 \\ 2.332 \cdot 10^4 & 8.565 \cdot 10^4 & -9.816 \cdot 10^3 \\ 9.816 \cdot 10^3 & -9.816 \cdot 10^3 & 4.25 \cdot 10^4 \end{bmatrix} \quad \left[\frac{N}{mm} \right]$$

$$B = \begin{pmatrix} 0 & 0 & 0 \\ 0 & 0 & 0 \\ 0 & 0 & 0 \end{pmatrix} \quad [N] \quad (A1.17)$$

$$D = \begin{bmatrix} 2.32 \cdot 10^3 & 485.741 & 668.068 \\ 485.741 & 1.249 \cdot 10^3 & 259.088 \\ 668.068 & 259.088 & 885.437 \end{bmatrix} \quad [N * mm]$$

Therefore:

$$\begin{pmatrix} A & B \\ B & D \end{pmatrix} = \begin{bmatrix} 8.565 \cdot 10^4 & 2.332 \cdot 10^4 & 9.816 \cdot 10^3 & 0 & 0 & 0 \\ 2.332 \cdot 10^4 & 8.565 \cdot 10^4 & -9.816 \cdot 10^3 & 0 & 0 & 0 \\ 9.816 \cdot 10^3 & -9.816 \cdot 10^3 & 4.25 \cdot 10^4 & 0 & 0 & 0 \\ 0 & 0 & 0 & 2.32 \cdot 10^3 & 485.741 & 668.068 \\ 0 & 0 & 0 & 485.741 & 1.249 \cdot 10^3 & 259.088 \\ 0 & 0 & 0 & 668.068 & 259.088 & 885.437 \end{bmatrix} \quad (A1.18)$$

Using the (A1.6) equation is possible to determine the strain vector imposing a traction force therefore:

$$\begin{pmatrix} N \\ M \end{pmatrix} = \begin{bmatrix} N_x \\ N_y \\ N_{xy} \\ M_x \\ M_y \\ M_{xy} \end{bmatrix} = \begin{bmatrix} 100 \\ 0 \\ 0 \\ 0 \\ 0 \\ 0 \end{bmatrix} \quad (A1.19)$$

$$\begin{pmatrix} \varepsilon^0 \\ \kappa \end{pmatrix} = \begin{bmatrix} \varepsilon_x^0 \\ \varepsilon_y^0 \\ \gamma_{xy}^0 \\ \kappa_x \\ \kappa_y \\ \kappa_{xy} \end{bmatrix} = \begin{pmatrix} A & B \\ B & D \end{pmatrix}^{-1} \cdot \begin{pmatrix} N \\ M \end{pmatrix} = \begin{bmatrix} 0.001 \\ -4.062 \cdot 10^{-4} \\ -3.996 \cdot 10^{-4} \\ 0 \\ 0 \\ 0 \end{bmatrix}$$

We have longitudinal deformation (in the direction of the force) accompanied by a lateral deformation in the opposite sense but there is also a negative shear strain. The deformed specimen is shown in figure A.2.

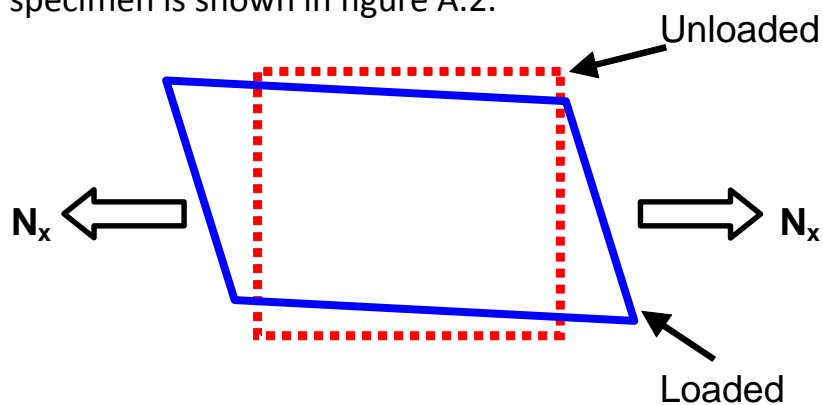


Figure A.2: Deformation of specimen discussed in case $(30^\circ/-60^\circ)_s$.

REFERENCES

- [1] David, R., "Problem solving with fortran 90".
- [2] ABAQUS/Standard User's Manual. Hibbit Karlson and Soresen Inc. (1998) Pawtucket RI.
- [3] Naik, R.A., "Analysis of Woven and Braided Fabric Reinforced Composites", NASA Contract Report CR-194930, 1994.
- [4] Reddy, J.N., "Mechanics of laminated composite plates and shells", CRC Press, 2004.
- [5] Tsai, S.W., "Theory of composites design", Think composites, 1992.
- [6] Moriani, A., "A method to represent the results about a progressive failure model in composite materials", 8th Seminar on Experimental Techniques and Design in Composite Materials – ETDCM8, 2007.
- [7] Takashi Nozawa et al., "Implementation report on preliminary Evaluation for the R&D on Mechanical Properties of SiC/SiC Composites", BA IFERC Project DEMO R&D Activities, 2009.